Mixed-Chain Phospholipids: Structures and Chain-Melting Behavior

Ching-hsien Huang*,[1]

Department of Biochemistry and Molecular Genetics, University of Virginia School of Medicine, Charlottesville, Virginia 22908

ABSTRACT: It has long been established that diacyl phospholipids isolated from animal cell membranes are predominantly of a mixed-chain variety, meaning that the *sn*-1 and *sn*-2 acyl chains are saturated and unsaturated acyl chains, respectively. In general, monoenoic and dienoic acids are found in the *sn*-2 acyl chain of phosphatidylcholine (PtdCho), whereas polyenoic acids are in phosphatidylethanolamine (PtdEth). These unsaturated chains contain only *cis*-double bonds, which are always methylene-interrupted. In recent years, the structures and the chain-melting behavior of mixed-chain PtdCho and PtdEth have been systematically studied in this laboratory. Specifically, we have examined the effects of chain unsaturation of the *sn*-2 acyl chain on the phase transition temperature (T_m) of many PtdCho and PtdEth by high-resolution differential scanning calorimetry (DSC). The T_m values, for instance, obtained from all-unsaturated mixed-chain PtdEth derived from a common precursor can be grouped together according to their chemical formula to form a T_m-diagram. Hence, all the T_m values can be compared simply, systematically, and simultaneously using the T_m-diagram. In addition, the energy-minimized structures of mixed-chain phospholipids containing different numbers/positions of methylene-interrupted *cis*-double bonds have been simulated by molecular mechanics calculations (MM). In this review, the results of our MM and DSC studies carried out with various mixed-chain phospholipids are summarized. In addition, we emphasize that the combined approach of MM and DSC yields unique information that can correlate the various T_m-profiles seen in the T_m-diagram with the structural variation of mixed-chain lipids as caused by the introduction of different numbers/positions of methylene-interrupted *cis*-double bonds.

Paper no. L8846 in *Lipids 36,* 1077–1097 (October 2001).

Diacyl phospholipids are amphipathic lipid molecules that can be found in all cell and organelle membranes. These lipid molecules serve not only as a basic structural component of cell and organelle membranes but also as the precursors in lipid-mediated signal transduction. In animal cells, membrane phospholipids are structurally an extremely diverse group of lipid molecules (Fig. 1) which includes principally phosphatidylcholine (PtdCho), phosphatidylethanolamine (PtdEth), phosphatidylinositol (PtdIns), phosphatidylglycerol (PtdGro), cardiolipin (Ptd_2Gro), and phosphatidylserine (PtdSer). Of these various classes, PtdCho and PtdEth are quantitatively the most

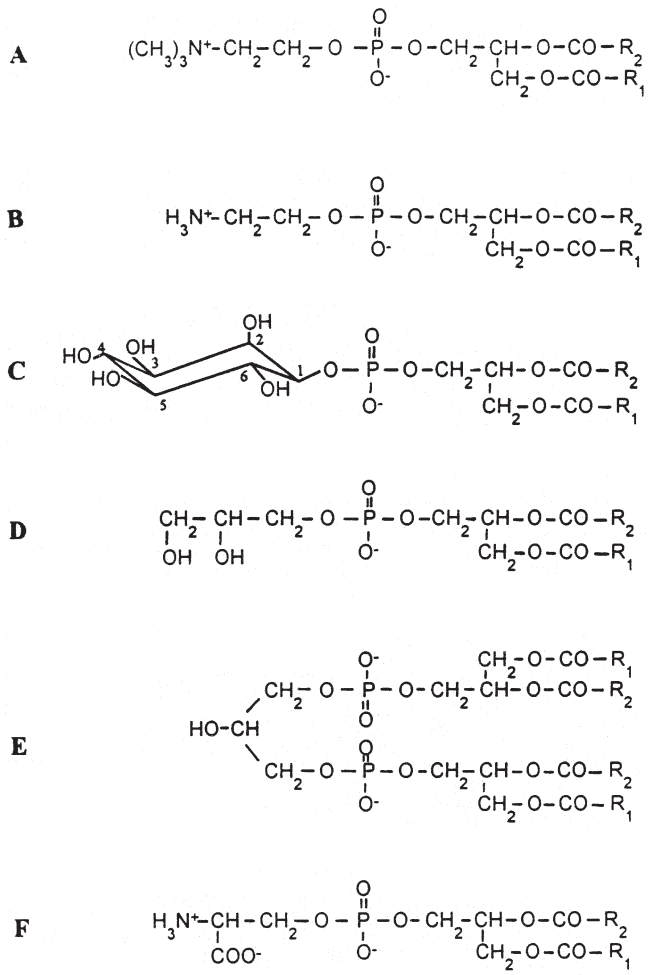

FIG. 1. The chemical formulas of diacyl phospholipids that are commonly found in membranes of animal cells. (A) Phosphatidylcholine (PtdCho), (B) phosphatidylethanolamine (PtdEth), (C) phosphatidylinositol (PtdIns), (D) phosphatidylglycerol (PtdGro), (E) diphosphatidylglycerol (Ptd_2Gro), and (F) phosphatidylserine (PtdSer). R_1 and R_2 refer to hydrocarbon chains of fatty acids esterified at carbons 1 and 2 of the glycerol backbone in diacyl phospholipids.

*E-mail: ch9t@unix.mail.virginia.edu

[1]Present address: 2537 Belgreen St., Las Vegas, NV 89135.

Abbreviations: ATS, all-*trans* segment; ΔC, effective chain length difference, as measured in C–C bonds, between the *sn*-1 and the *sn*-2 acyl chains, an indication of chain asymmetry; ΔC_{ref}, effective chain length difference of the reference state [or, effective chain length difference between the *sn*-1 and *sn*-2 acyl chains]; CL, effective chain length of the longer of the two acyl chains; DSC, differential scanning calorimetry; MM, molecular mechanics; N, distance, in C–C bond lengths, between the two carbonyl oxygens of the *sn*-1 acyl chains in a trans-bilayer dimer of C(X):C(Y)PtdCho; PtdCho, phosphatidylcholine; PtdEth, phosphatidylethanolamine; PtdGro, phosphatidylglycerol; Ptd_2Gro, cardiolipin (= diphosphatidylglycerol); PtdIns, phosphatidylinositol; PtdSer, phosphatidylserine; T_m, main phase transition temperature.

important species. The basic structure of a given class of diacyl phospholipids has customarily been considered to consist of three regions: the polar headgroup, the interfacial region, and the hydrocarbon tail. As shown in Figure 1, the structural features that are common to all classes of phospholipids are the tetrahedrally arranged phosphorus atom in the polar headgroup, the glycerol backbone moiety in the interfacial region, and the long fatty acyl chains in the hydrocarbon tail (1).

In most animal cells, diacyl phospholipids are predominantly of a mixed-chain variety, meaning that the two acyl chains are structurally different. Specifically, the two fatty acids esterified at the *sn*-1 and *sn*-2 positions of the glycerol backbone are originated *in vivo* from saturated and unsaturated fatty acyl-CoA, respectively (2). In particular, the saturated *sn*-1 acyl chain contains an even number of carbon atoms ranging from 14 to 22, predominantly 16 and 18 carbons. The unsaturated *sn*-2 acyl chain may have 16–22 carbons; in addition, it contains 1–6 *cis*-double bonds (Δ-bonds). Interestingly, two or more Δ-bonds in the *sn*-2 acyl chains are always methylene-interrupted, indicating that two neighboring *cis*-double bonds are invariably separated from each other in the *sn*-2 acyl chain by a methylene unit (3). It should be pointed out that (i) methylene-interrupted *cis*-double bonds are the hallmark of membrane lipids originated from animal cells, and (ii) these structural elements are absent in other basic biological molecules such as protein, nucleic acid, and carbohydrate.

Over the last several decades, a wide variety of biochemical and biophysical studies have offered productive approaches for investigating the structure, dynamics, and properties of membrane phospholipids self-assembled, in excess H_2O, in the lipid bilayer (4,5). Most of these studies have been concerned with synthetic phospholipids that contain two identical saturated fatty acids. Occasionally, mixed-chain phospholipids containing various polyenoic fatty acids at the *sn*-2 position have been studied (6–12). These studies have been concerned exclusively with mixed-chain PtdCho. In biological membranes, however, mixed-chain PtdCho usually contain one or two Δ-bonds in the *sn*-2 acyl chains. In contrast, polyenoic fatty acids are present most abundantly in mixed-chain PtdEth. Consequently, our current knowledge about the structural and physicochemical properties of naturally occurring phospholipids, particularly mixed-chain PtdEth with saturated *sn*-1 and polyunsaturated *sn*-2 acyl chains, is limited. To approach a broader understanding of the structures/properties of naturally occurring phospholipids, we have in recent years synthesized a large number of mixed-chain phospholipids, including PtdCho, PtdEth, PtdGro, and phosphatidylethanol, that have the same structures as those of naturally occurring phospholipids (13,14). Specifically, these synthesized mixed-chain phospholipids contain the same number and position of methylene-interrupted *cis*-double bonds in the *sn*-2 acyl chain as those that are commonly found in membrane phospholipids of animal cells. Subsequently, we have carried out a systematic and comprehensive study of the structure/chain-melting behavior of the lipid bilayer comprised of the synthesized mixed-chain phospholipids. In these studies, computational molecular mechanics (MM) simulations and differential scanning calorimetry (DSC) are employed. I shall summarize some of our recent studies obtained with mixed-chain PtdCho and PtdEth in this review. These studies give unique information relating the energy-minimized structures of mixed-chain PtdCho and PtdEth to the chain-melting behavior of lipid bilayers composed of the corresponding PtdCho and PtdEth.

THE STRUCTURE AND PHASE TRANSITION BEHAVIOR OF SATURATED C(X):C(Y)PtdCho

To examine the structure and the chain-melting behavior of the lipid bilayer composed of mixed-chain phospholipids with saturated *sn*-1 and unsaturated *sn*-2 acyl chains, let us first examine the structure and the chain-melting behavior of saturated mixed-chain phospholipids such as C(X):C(Y)PtdCho packed in the lipid bilayer. Here, the abbreviation C(X) designates the total number of carbons in the *sn*-1 acyl chain and C(Y) designates the total number of carbons in the *sn*-2 acyl chain. Both the *sn*-1 and *sn*-2 acyl chains contain only saturated hydrocarbon chains.

Figure 2 shows the energy-minimized structure of C(16):C(16)-PtdCho obtained with MM calculations using Allinger's MM3(92) program (15). The atomic coordinates used as the initial input for MM calculations were derived from experimental data obtained by x-ray diffraction (16). Two conformational features of the acyl chains are revealed by the energy-minimized structure. First, the fully extended *sn*-1 and *sn*-2 acyl chains are aligned in the same direction; however, the zigzag planes of the *sn*-1 and *sn*-2 acyl chains are oriented perpendicularly to each other. Second, although the *sn*-1 and *sn*-2 acyl chains have the same total number of methylene units, there is an effective chain length difference between them. This is due largely to the fact that the *sn*-2 acyl chain is bent 90° at C(2). It should be pointed out that the energy-minimized structure corresponds to the structure of lipid packed in the crystalline state. In the gel-state bilayer, the *sn*-2 acyl chain of C(16):C(16)PtdCho is still bent; however, the effective chain length difference between the *sn*-1 and the *sn*-2 acyl chains is smaller, and, is about 1.5 C–C bond lengths according to neutron diffraction measurements (17). This value can be applied to all saturated identical-chain PtdCho packed in the gel-state bilayer, and we designate it as ΔC_{ref}, the effective chain length difference of the reference state, as shown in Figure 2. The effective chain length of the longer of the two acyl chains (CL) is also introduced in Figure 2. In the case of C(16):C(16)PtdCho packed in the gel-state bilayer, the value of CL is 15 C–C bond lengths, which corresponds to the effective chain length of the *sn*-1 acyl chain.

For saturated mixed-chain C(X):C(Y)PtdCho packed in the gel-state bilayer, three structural parameters are graphically illustrated in Figures 3A and 3B (13). ΔC is the effective chain length difference, in C–C bond lengths, between the *sn*-1 and the *sn*-2 acyl chains. It represents the chain asymmetry. The larger the ΔC value, the greater the asymmetry of the lipid's

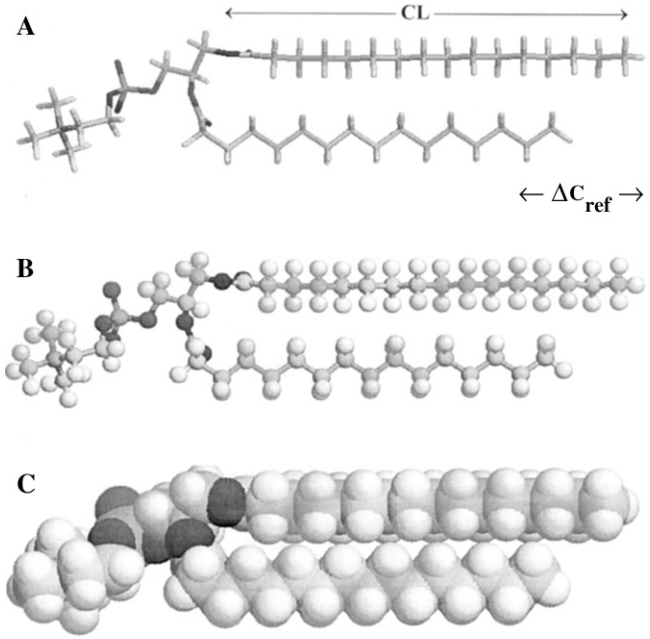

FIG. 2. The energy-minimized structure of C(16):C(16)PtdCho obtained by molecular mechanics simulations. This structure corresponds to C(16):C(16)PtdCho packed in the crystalline bilayer. The structural parameter ΔC_{ref} refers to the effective chain length difference between the *sn*-1 and the *sn*-2 acyl chains, which is about 1.5 C–C bond length for C(16):C(16)PtdCho packed in the gel-state bilayer. This value can, in fact, be applied to all saturated identical-chain PtdCho packed in the gel-state bilayer; hence, ΔC_{ref} is the effective chain length difference of the reference state. A second structural parameter, CL, refers to the effective chain length of the longer of the two acyl chains. In the case of C(16):C(16)PtdCho packed in the gel-state bilayer, the chain length difference between the two acyl chains, ΔC_{ref}, is 1.5 C–C bond lengths, and the length of the longer chain, CL = X – 1, is 15 C–C bond lengths, or 19 Å, which corresponds to the effective chain length of the *sn*-1 acyl chain. The normalized chain length difference, ΔC_{ref}/CL, is 0.10.

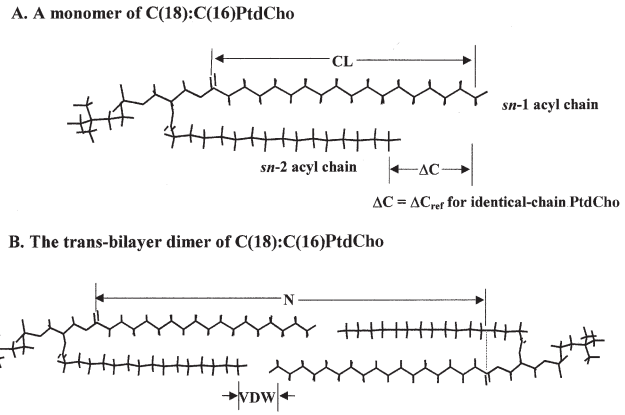

FIG. 3. A molecular-graphically depicted diagram illustrating the various structural parameters (ΔC, CL, and N) of C(18):C(16)PtdCho. (A) A monomer of C(18):C(16)PtdCho. ΔC is the effective chain length difference between the two acyl chains along the long molecular axis. The units for ΔC are carbon-carbon bond lengths. ΔC_{ref} is the ΔC value for identical-chain PtdCho packed in the gel-state bilayer, and ΔC_{ref} is taken to be 1.5 C–C bond lengths. For C(X):C(Y)PtdCho packed in the gel-state bilayer, $\Delta C = |X - Y + \Delta C_{ref}| = |X - Y + 1.5|$. In the case of C(18):C(16)PtdCho, the value of ΔC is 3.5 C–C bond lengths. CL is the effective length of the longer chain of the two acyl chains, also in units of C–C bond lengths. In the case of C(18):C(16)PtdCho, the value of CL is 17. (B) The trans-bilayer dimer of C(18):C(16)PtdCho with a partially interdigitated packing motif at $T < T_m$, where T is the experimental temperature and T_m is the main phase transition temperature. N is the effective hydrophobic thickness of the dimer, corresponding to the separation distance between the two carbonyl oxygens of the *sn*-1 acyl chains in the two opposing leaflets of the bilayer. VDW is the van der Waals contact distance between the two opposing methyl termini in the bilayer interior, and is assumed to be 3 C–C bond lengths in the gel-state bilayer. The structural parameter N is related to X and Y in C(X):C(Y)PtdCho as follows: N = (X – 1) + VDW + (Y – 2.5) = X + Y – 0.5. For the gel-state bilayer of C(18):C(16)PtdCho, the value of N is 33.5 C–C bond lengths.

acyl chains. The second structural parameter, CL, has the same meaning as that illustrated for C(16):C(16)PtdCho shown in Figure 2. The distance N, in C–C bond lengths, between the two carbonyl oxygens of the *sn*-1 acyl chains in a trans-bilayer dimer of C(X):C(Y)PtdCho is introduced in Figure 3B. N represents the effective hydrocarbon-core thickness of the lipid bilayer composed of C(X):C(Y)PtdCho. These three structural parameters, in C–C bond lengths, are related to X and Y in C(X):C(Y)PtdCho as follows (13):

$$\Delta C = |X - Y + \Delta C_{ref}| \quad [1]$$

$$CL = (X - 1) \quad [2]$$

$$N = X + Y - 0.5 \quad [3]$$

The crystalline structure of C(X):C(Y)PtdCho, as represented by C(18):C(16)PtdCho, is drawn in Figure 3 for the purpose of simplicity. All three structural parameters are actually defined for C(X):C(Y)PtdCho packed in the gel-state bilayer with a partially interdigitated packing motif. In this packing motif, the methyl terminus of the *sn*-1 acyl chain of one lipid molecule in the bilayer is juxtaposed with the methyl end of the *sn*-2 acyl chain of another lipid molecule from the opposing bilayer leaflet as shown diagrammatically in Figure 3B. It is well established that C(X):C(Y)PtdCho with ΔC/CL < 0.42 can, in excess water, self-assemble into the partially interdigitated bilayer at $T < T_m$ where T = experimental temperature and T_m = main phase transition temperature (18).

Figure 4 shows some representative DSC curves obtained with aqueous lipid dispersions prepared from a homologous series of mixed-chain C(X):C(Y)PtdCho. These mixed-chain lipids share a common value of (X + Y), which corresponds to 32 carbons (19). Hence, the N value for the gel-state bilayer prepared from each lipid species of this lipid series is identical. However, the ΔC value obtained with each lipid in this series increases stepwise by 1.0 C–C bond length as the lipid species changes progressively from C(15):C(17)PtdCho to C(10):C(22)PtdCho. Figure 4 clearly shows that the T_m exhibited by C(X):C(Y)PtdCho with ΔC/CL < 0.42 decreases steadily as the value of ΔC increases. This figure demonstrates that, for a series of C(X):C(Y)PtdCho packed in the partially interdigitated bilayer, T_m decreases with increasing ΔC value when N is held constant. In addition, for a homologous series of saturated identical-chain PtdCho (ΔC/CL < 0.42), ranging from C(13):C(13)PtdCho to C(21):C(21)PtdCho, with a common ΔC

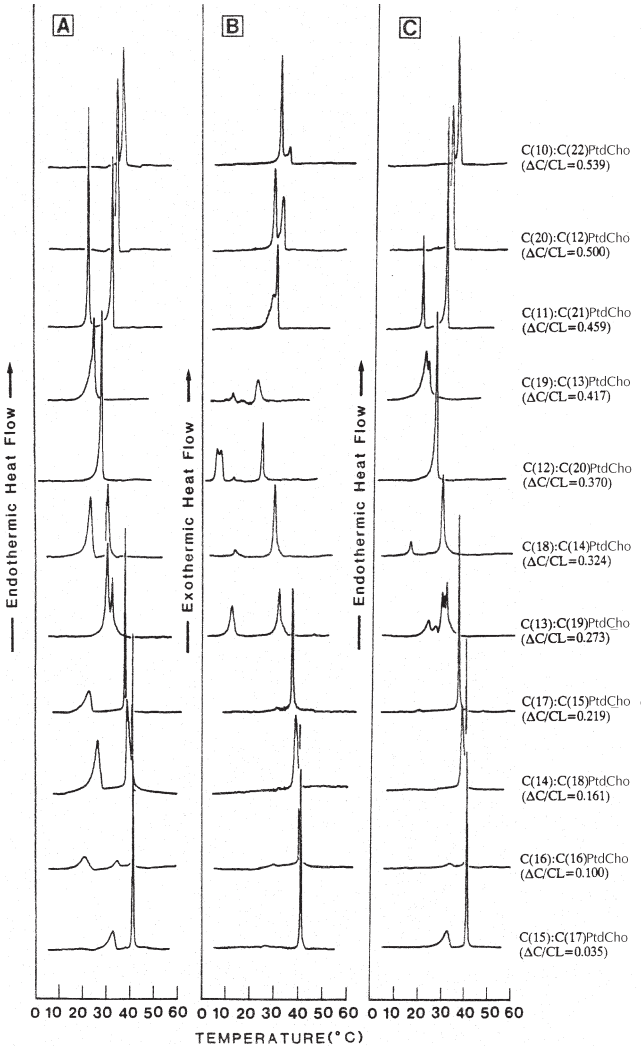

FIG. 4. The differential scanning calorimetry (DSC) curves obtained with aqueous lipid dispersions prepared from a homologous series of mixed-chain C(X):C(Y)PtdCho. These mixed-chain lipids share a common value of (X + Y), which corresponds to 32 carbons. The ΔC/CL represents the normalized chain length difference. (A) The initial heating scans, (B) the first cooling scans, and (C) the second heating scans. The DSC scans were obtained from a Microcal MC-2 microcalorimeter (Microcal, Inc., Northampton, MA). Scan rate: 15°C/h. Prior to DSC experiments, each lipid sample was incubated at 0°C for a minimum of 24 h. For abbreviations see Figures 1 and 3.

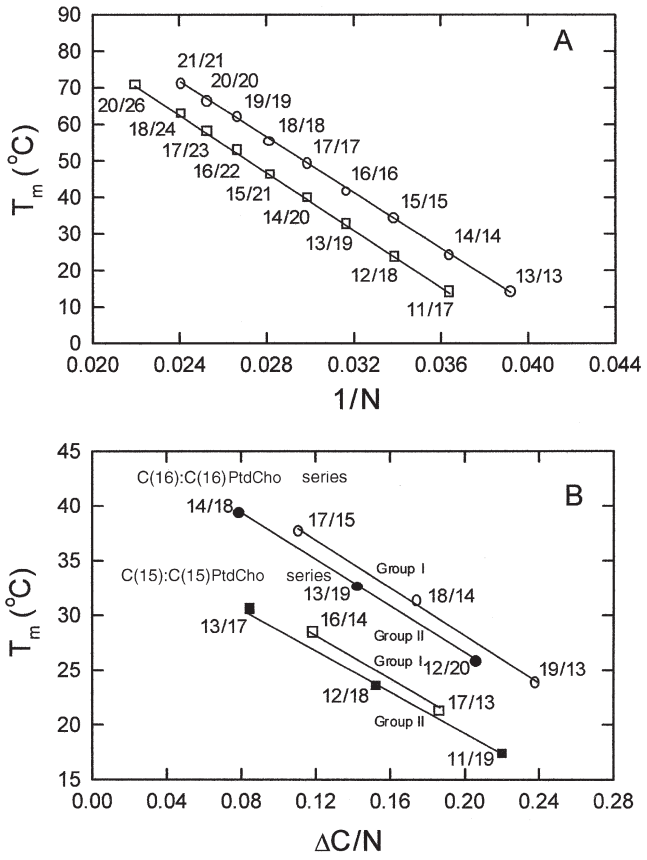

FIG. 5. Plots of the phase transition temperature, T_m, vs. the structural parameter(s). (A) T_m values from two series of saturated PtdCho with ΔC = 1.5 and 4.5, respectively, are plotted against 1/N. The numerical numbers of X/X or X/Y next to the data points denote the numbers of carbons in the *sn*-1/*sn*-2 acyl chains of the corresponding phosphatidylcholine species. (B) T_m values of lipids with identical N values vs. ΔC/N. The data (○,●) connected by the top two lines were obtained with saturated PtdCho having a constant N value of 31.5 C–C bond lengths. These lipids thus belong to the C(16):C(16)PtdCho series. The data (□,■) in the bottom two lines were obtained with saturated PtdCho having a constant N value of 29.5 C–C bond lengths; hence, these lipids belong to the C(15):C(15)PtdCho series. Within each series, lipids with an effective longer *sn*-1 acyl chain length (X ≥ Y – 1.5) are grouped into Group I lipids, and those with longer effective *sn*-2 acyl chain (Y – 1.5 > X) are classified as Group II lipids.

value of 1.5 C–C bond lengths, the T_m value exhibited by the lipid dispersion prepared individually from them decreases as the value of 1/N increases (Fig. 5). Moreover, the same trend is observed in Figure 5 for another homologous series of mixed-chain C(X):C(X + 6)PtdCho (ΔC/CL < 0.42) with a common ΔC value of 4.5 C–C bond lengths (20). Based on DSC data presented in Figure 5 and elsewhere, the T_m value of C(X):C(Y)-PtdCho (ΔC/CL < 0.42) with X ≥ Y can be related to the structural parameters ΔC and N in a simple first-order manner (13):

$$T_m = 161.75 - 3706.06\,(1/N) - 278.75\,(\Delta C/N) + 239.94\,[\Delta C/(N + \Delta C)] \quad [4]$$

A similar equation (Eq. 5) is also derived for C(X):C(Y)-PtdCho with X < Y (13):

$$T_m = 155.11 - 3534.31(1/N) - 245.78(\Delta C/N) + 199.04\,[\Delta C/(N + \Delta C)] \quad [5]$$

These two equations not only show the fundamental antagonistic effect between N and ΔC in determining the T_m value but also can be employed to predict the T_m value for C(X):C(Y)PtdCho with ΔC/CL < 0.42. The prediction of T_m value based on the chemical formula of C(X):C(Y)PtdCho is possible because the N and ΔC values can be readily calculated from X and Y (Eqs. 1–3). Predicted T_m values (n = 207) for various C(X):C(Y)PtdCho, obtained on the basis of Equations 4 and 5, are presented in Table 1, along with 54 T_m values observed calorimetrically. Clearly, the predicted and the observed T_m values agree well. An important consequence of this excellent agreement is that the number of carbon atoms in the *sn*-1 (or *sn*-2) acyl chain, X (or Y), can be determined

TABLE 1
Predicted T_m Values for Fully Hydrated Samples of Saturated Diacyl C(X):C(Y)PtdCho with Varying Degrees of Acyl Chain Length Asymmetry[a]

Total carbons in the *sn*-1 acyl chain	Total carbons in the *sn*-2 acyl chain																	
	9	10	11	12	13	14	15	16	17	18	19	20	21	22	23	24	25	26
26												68.3	72.5	76.4	79.8	83.0	85.9	88.5
25											63.8	68.3	72.5	76.2	79.7	82.7	85.5	88.0
24										58.8	63.7	68.2	72.3	76.0	79.3	82.3	84.9	83.2
23									53.3	58.7	63.6	68.0	72.0	75.6	78.8	81.6	80.2	80.6
22								47.2	53.1	58.4	63.3	67.6	71.5	74.9	78.0	76.9	77.4	77.7
														74.8				***77.8***
21							40.3	46.8	52.7	58.0	62.8	67.0	70.7	74.1	73.3	73.9	74.3	74.5
													71.1					
20						32.6	39.9	46.4	52.2	57.4	62.0	66.1	69.7	69.3	70.1	70.5	70.9	71.0
						33.2				56.8		***66.4***						***70.7***
19						32.0	39.2	45.7	51.4	56.5	61.0	64.9	65.0	65.8	66.4	66.8	67.1	67.2
						31.8	***39.0***				***61.8***							
18					23.0	31.1	38.3	44.7	50.3	55.3	59.6	60.2	61.2	61.9	62.4	62.8	62.9	63.0
						31.2	***38.1***	***44.4***	***50.4***	***55.3***		***59.7***		***62.2***		***62.7***		***63.9***
17					21.9	30.0	37.1	43.4	48.9	53.7	54.8	56.0	56.9	57/5	58.0	58.3	58.4	58.4
					21.2		***37.7***	***43.2***	***49.0***						***57.9***			
16				11.2	20.4	28.5	35.6	41.7	47.1	48.9	50.3	51.3	52.1	52.7	53.1	53.3	53.4	53.4
				11.3		***28.4***		***41.4***	***46.2***	***48.8***				***52.8***		***53.2***		***53.3***
15			–1.1	9.4	18.6	26.6	33.6	39.5	42.1	43.8	45.1	46.1	46.8	47.3	47.7	47.9	48.0	
					18.8		***34.0***		***41.7***		***44.8***		***46.1***					
14		–15.7	–3.5	7.1	16.3	24.2	31.0	34.5	36.5	38.0	39.2	40.2	40.8	41.3	41.7	41.9		
						24.1	***30.7***	***34.9***		***39.2***		***39.8***				***43.3***		
13		–18.7	–6.4	4.3	13.3	21.1	25.7	28.1	30.0	31.5	32.7	33.6	34.3	34.8				
					13.9		***25.8***		***30.5***		***32.6***	***33.1***	***34.1***					
12		–22.4	–9.9	0.7	9.6	15.5	18.5	20.8	22.7	24.2	25.3	26.2						
								21.7		***23.5***		***25.6***						
11	–41.8	–26.9	–14.4	–3.9	3.6	7.3	10.2	12.5	14.4	15.9	17.1							
									13.9		***17.3***							
10	–47.7	–32.6	–20.1	–10.5	–5.9	–2.3	0.6	3.0	4.9									
9	–55.0	–39.8	–27.5	–21.7	–17.1	–13.4	–10.4											

[a]Experimental T_m values are also indicated in boldface italic. Predicted T_m values are calculated in part from Equation 4 (see text) and the relationships between ΔC, N, X, and Y as indicated in Figure 3. Abbreviations: PtdCho, phosphatidylcholine; T_m, main phase transition temperature; ΔC, effective chain length difference as measured in C–C bonds; N, distance, in C–C bond lengths, between the two carbonyl oxygens of the *sn*-1 acyl chains in a trans-bilayer dimer of C(X):C(Y)phosphatidylcholine; X, total carbons in the *sn*-1 acyl chain; Y, total carbons in the *sn*-2 acyl chain.

accurately provided that the T_m value and the number of carbon atoms in the *sn*-2 (or *sn*-1) acyl chain, Y (or X), of C(X):C(Y)PtdCho are known. This important relationship will be reiterated later when I discuss the structure/chain-melting behavior of mixed-chain lipids with saturated *sn*-1 and unsaturated *sn*-2 acyl chains.

THE STRUCTURES AND THE PHASE TRANSITION BEHAVIOR OF PtdCho AND PtdEth WITH SATURATED *sn*-1 AND MONOUNSATURATED *sn*-2 ACYL CHAINS [C(X):C(Y:1Δ^n)PtdCho AND C(X):C(Y:1Δ^n)PtdEth]

The six atoms in the immediate vicinity of a *cis*-double bond, C–CH=CH–C, in a long hydrocarbon chain are coplanar (Fig. 6). Although the rotational flexibility of the *cis*-double bond is highly restricted at physiological temperatures, paradoxically the carbon-carbon single bond preceding or succeeding the *cis*-double bond is rotationally highly flexible, even at –10°C (18). Results of our MM calculations indicate that the carbon-carbon single bond next to the *cis*-double bond prefers to adopt the *skew* ($s^{\pm}$) conformation with torsion angle of about ±110° (Fig. 6). As a result, the most stable structure of a hydrocarbon chain containing a single *cis*-double bond has a twisted boomerang-like conformation with a $s^{\pm}\Delta s^{\pm}$ sequence around the Δ-bond (Fig. 7). Such a twisted boomerang-like conformation, however, is unlikely to be adopted by the *sn*-2 acyl chain in the gel-state bilayer composed of monounsaturated mixed-chain lipids because the all-*trans sn*-1 acyl chain would impose steric constraints on the boomerang-like conformation of the neighboring *sn*-2 acyl chain. Results from our detailed MM calculations indicate that in the presence of an all-*trans sn*-1 acyl chain, the *sn*-2 acyl chain of the monoenoic PtdCho is able to pack favorably in the gel-state bilayer with a kinked crankshaft-like conformation (18,21). Specifically, two parallel chain segments separated by a small kink sequence are observed in this kinked *sn*-2 acyl chain; moreover, these two parallel segments are in close van der Waals contact with the all-*trans sn*-1 acyl chain.

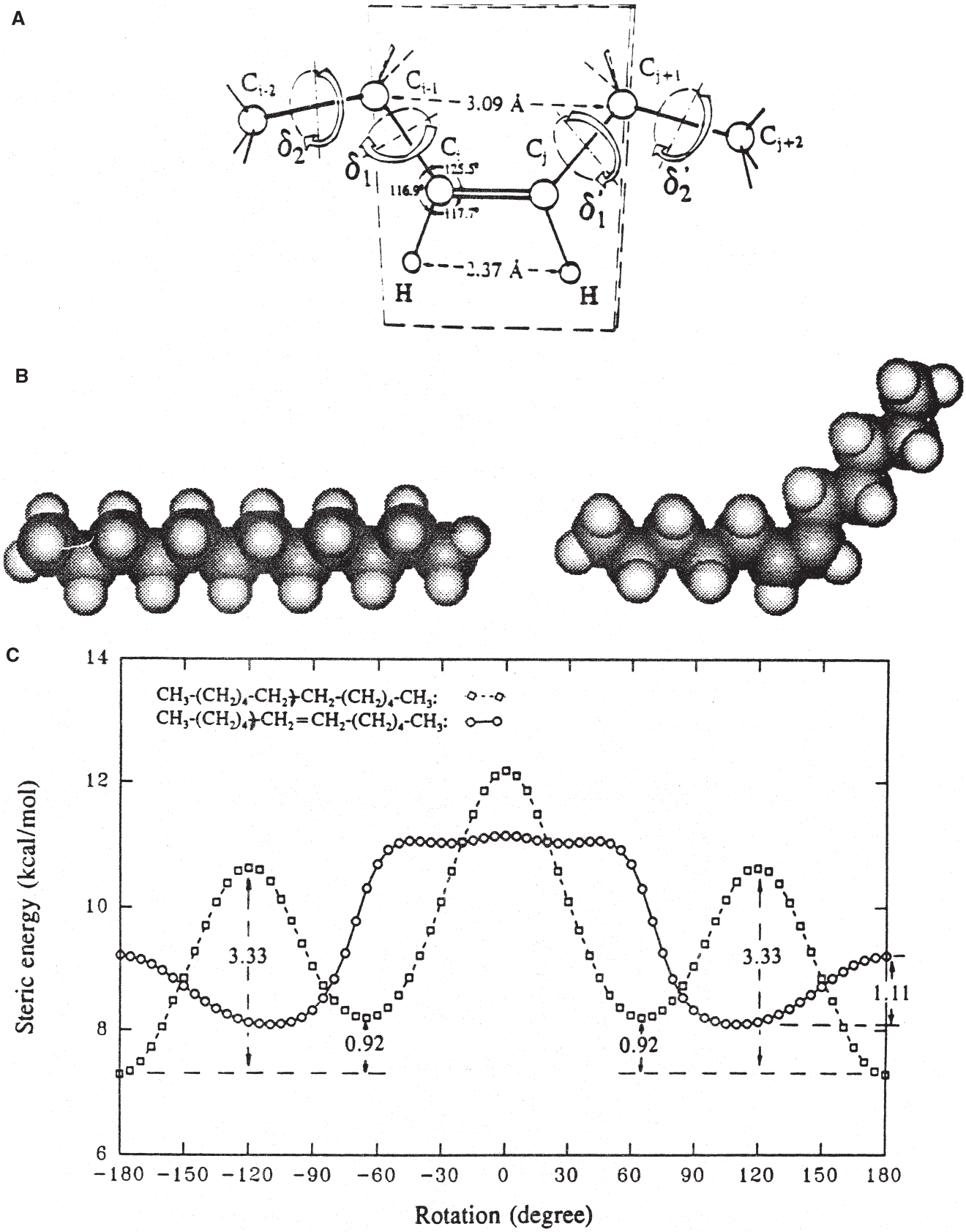

FIG. 6. Structure of a *cis*-double bond in a segment of hydrocarbon chain is shown in the top (A). The introduction of a *cis*-double bond into an all-*trans* hydrocarbon chain transforms the linear conformation into a boomerang-like conformation (B). In (C) the energy profiles arising from rotations of a single C(6)-C(7) bond in dodecane (□) and of a single C(4)-C(5) bond in dodecene-6 (○) are shown. Molecular mechanics (MM) calculations were performed with the MM2(85) program (15).

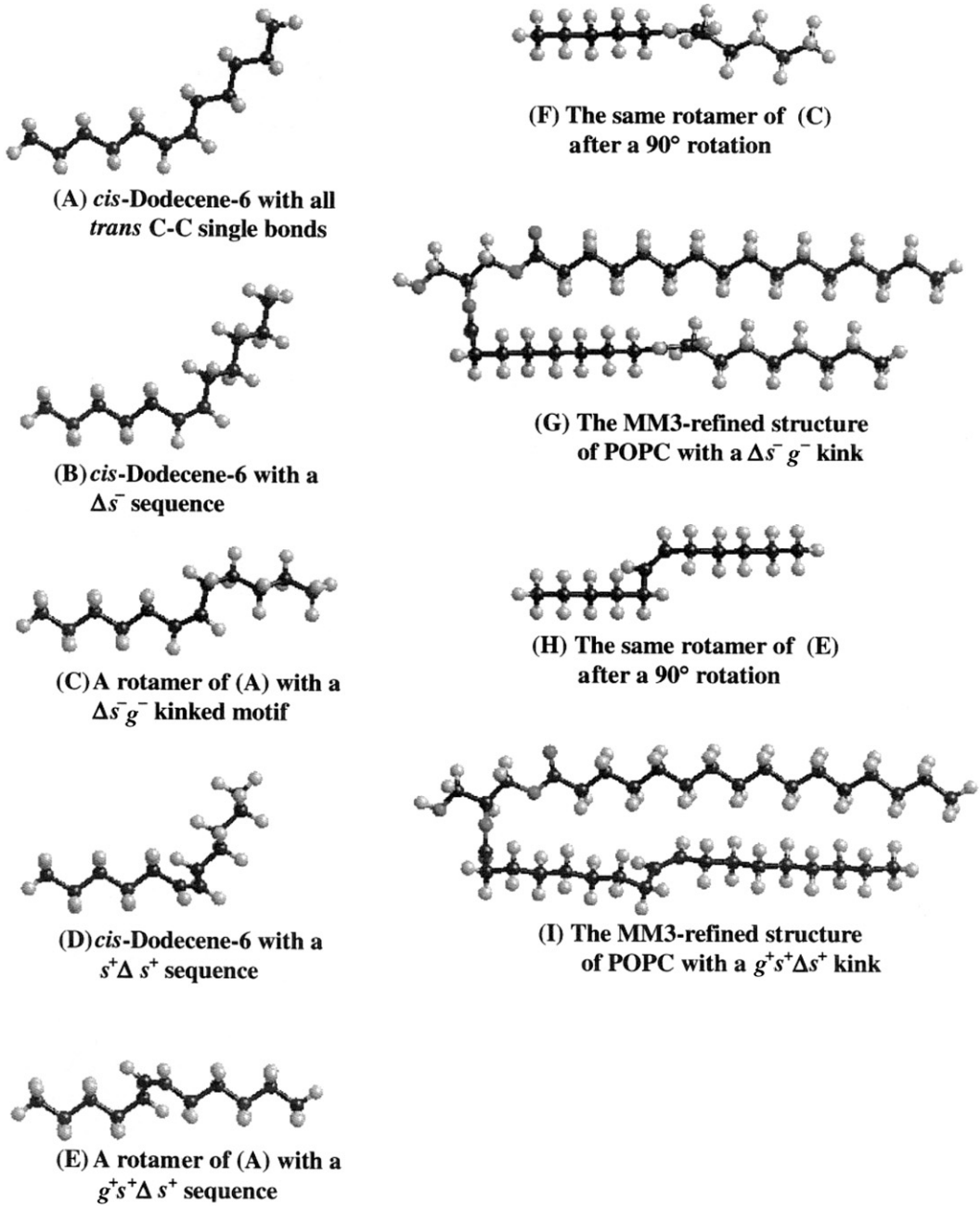

FIG. 7. Computer-graphic representations of the hydrocarbon chain with boomerang-like, twisted boomerang-like, and kinked crankshaft-like motifs. Two kinked conformations with identical low-energy for C(16):C(18:1Δ^9)PtdCho as obtained by MM calculations are also shown. POPC, 1-palmitoyl-2-oleoyl-PtdCho; for other abbreviations see Figures 1 and 6.

As a result, such a kinked motif has a low steric energy. As illustrated in Figure 7, a monoenoic hydrocarbon chain with kinked crankshaft-like conformation can be readily obtained by the rotational *trans* → *gauche* isomerizations of the C–C single bond next to the twisted boomerang sequence of $s^{\pm}\Delta s^{\pm}$. However, the overall length of the kinked chain is shortened by 0.8 C–C bond length relative to its saturated all-*trans* counterpart. Two of the kinked crankshaft-like lipid structures obtained with C(16):C(18:1Δ^9)PtdCho, 1-palmitoyl-2-oleoyl-phosphatidylcholine, are also illustrated in Figure 7. Here, the abbreviation C(18:1Δ^9) denotes the *sn*-2 acyl chain with a single *cis*-double bond at the ninth carbon (Δ^9) counting from the carbonyl end. In fact, we have shown by MM calculations that 16 kinked crankshaft-like conformations with a similar low steric-energy may exist normally for C(16):C(18:1Δ^9)-PtdCho at $T < T_m$ (18). Our MM calculations thus indicate that many possible low-energy rotational isomers (rotamers) may be adopted by monounsaturated PtdCho, and these rotamers are likely to interconvert rapidly in the bilayer at $T < T_m$. In addition, these low-energy rotamers share a common structural feature characterized by a kinked crankshaft-like motif.

Examining some representative DSC curves exhibited by lipid bilayers composed of monounsaturated phospholipids demonstrates an interesting point (21,22). In Figure 8, the second DSC heating curves obtained with aqueous dispersions of C(20):C(18)PtdCho, C(20):C(18)PtdEth, C(20):C(18:1Δ^9)-PtdCho, and C(20):C(18:1Δ^9)PtdEth in the presence of 50 mM NaCl, 5 mM phosphate buffer (pH 7.4), and 1 mM EDTA are illustrated (13). A sharp, single endothermic transition with T_m = 75.8°C is observed for C(20):C(18)PtdEth. The introduction of a single Δ^9-bond into the *sn*-2 acyl chain reduces the T_m value of C(20):C(18:1Δ^9)PtdEth to 33.9°C. As shown in Figure 8, this T_m-lowering effect of acyl chain monounsaturation is also observed for mixed-chain PtdCho. In particular, the T_m values exhibited by C(20):C(18)PtdCho and C(20):C(18:1Δ^9)PtdCho bilayers are 56.8 and 11.0°C, respectively, showing a marked reduction of 45.8°C in T_m as a single Δ^9-bond is introduced into the *sn*-2 acyl chain of C(20):C(18)PtdCho. Such a T_m-lowering effect of acyl chain monounsaturation has been previously observed for PtdCho by other investigators (8,12) but not for PtdEth.

Another distinct characteristic associated with the acyl chain monounsaturation is the T_m-lowering effect of acyl chain unsaturation, which is critically dependent on the position of the single *cis*-double bond along the *sn*-2 acyl chain (21). The second DSC heating curves for a series of C(18):C(18:1Δ^n)PtdCho with n = 6, 7, 9, 11, 12, and 13 demonstrate this point (Fig. 9). The minimal T_m is observed when n = 11 or when the *cis*-double bond is positioned near the center of the linear segment of the *sn*-2 acyl chain. Further, the T_m value increases progressively as the *cis*-double bond moves away from Δ^{11} toward either end of the acyl chain. Specifically, the T_m values of C(18):C(18:1Δ^n)PtdCho with n = 6, 7, 9, 11, 12, and 13 are 24.8, 16.7, 5.6, 3.8, 9.1, and 15.9°C, respectively. As a result, when T_m is plotted against the position of the single *cis*-double bond, a V-shaped T_m-profile is seen for the various positional isomers of C(18):C(18:1Δ^n)PtdCho. The second DSC heating curves for C(20):C(20:1Δ^n)PtdCho with n = 5, 8, 11, and 13 are also presented in Figure 9 (21). These data have been extended recently (23). The T_m values of lipid bilayers prepared from C(20):C(20:1Δ^n)PtdCho with n = 5, 8, 11, 13, and 17 are 44.9, 30.6, 19.4, 22.1, and 49.7°C, respectively. Again, a roughly V-shaped T_m-profile is observed in the plot of T_m vs. the position of the *cis*-double bond in the *sn*-2 acyl chain for this series of C(20):C(20:1Δ^n)PtdCho (23). Similarly, positional isomers of C(18:1Δ^n):C(18:1Δ^n)PtdCho also display a V-shaped T_m-profile in which a *cis*-double bond is present in each of the two acyl chains at the same position (6).

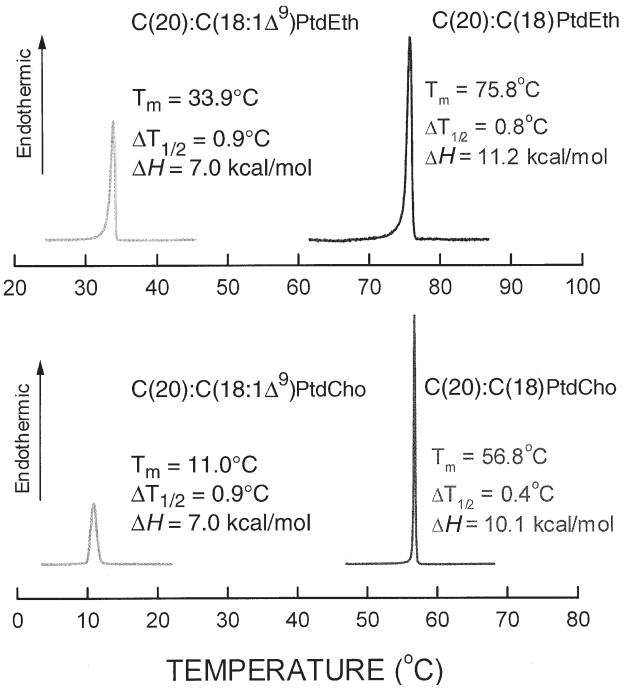

FIG. 8. The second DSC heating curves obtained with aqueous dispersions of C(20):C(18)PtdCho, C(20):C(18)PtdEth, C(20):C(18:1Δ^9)PtdCho, and C(20):C(18:1Δ^9)PtdEth. $\Delta T_{1/2}$ represents width of phase transition curve at half-peak height. Scan rate: 15°C/h. Lipid concentration: 3–5 mM. For abbreviations see Figure 1.

Before a molecular model that explains the effects of chain monounsaturation on phospholipids phase transition behavior is presented, let us first examine the energy-minimized structures of some saturated and monounsaturated phospholipids obtained with MM calculations (Figs. 10 and 11). First, compare the monomeric structures of C(18):C(18)PtdCho, C(18):C(17)PtdCho, and C(18):C(18:1Δ^{11})PtdCho. Clearly, the two acyl chains are more symmetrical, in terms of chain lengths, for C(18):C(18)PtdCho. Quantitatively, the chain-asymmetry parameter, ΔC, is nearly the same for C(18):C(17)PtdCho and C(18):C(18:1Δ^{11})PtdCho. Based on the relationship between ΔC and T_m that is known for saturated mixed-chain PtdCho, one would expect the values of T_m exhibited by C(18):C(17)PtdCho and C(18):C(18:1Δ^{11})-PtdCho to be nearly the same. Yet, the T_m value observed calorimetrically for C(18):C(18:1Δ^{11})PtdCho is 46.6°C smaller than for C(18):C(17)PtdCho. In comparing the *trans*-dimeric structures of C(18):C(17)PtdCho and C(18):C(18:1Δ^{11})-PtdCho, the overall *trans*-bilayer thickness is almost indistinguishable, with the structural parameter N being 34.5 and 34.7 C–C bond lengths, respectively. Again, based on the relationship between N and T_m that is known for saturated mixed-chain PtdCho, we would expect a nearly identical value of T_m for these two lipid species. This expectation, however, is not borne out by experimental data as shown in Figure 11. The phase transition behavior observed for unsaturated lipids is thus distinctively different from that of saturated lipids. Therefore, prediction of the chain-melting behavior of unsaturated lipids based solely on the chain-melting behavior of the corresponding saturated lipids cannot be made reliably.

Earlier, it was shown that the T_m value of saturated mixed-chain C(X):C(Y)PtdCho can be quantitatively related to X and Y values (Table 1). Similarly, the value of Y can also be calculated provided that T_m and X are known. The values of T_m and X for C(18):C(18:1Δ^{11})PtdCho are 3.8°C and 18, respectively. A corresponding saturated mixed-chain PtdCho with a partially interdigitated packing motif can thus be calculated; this fictive

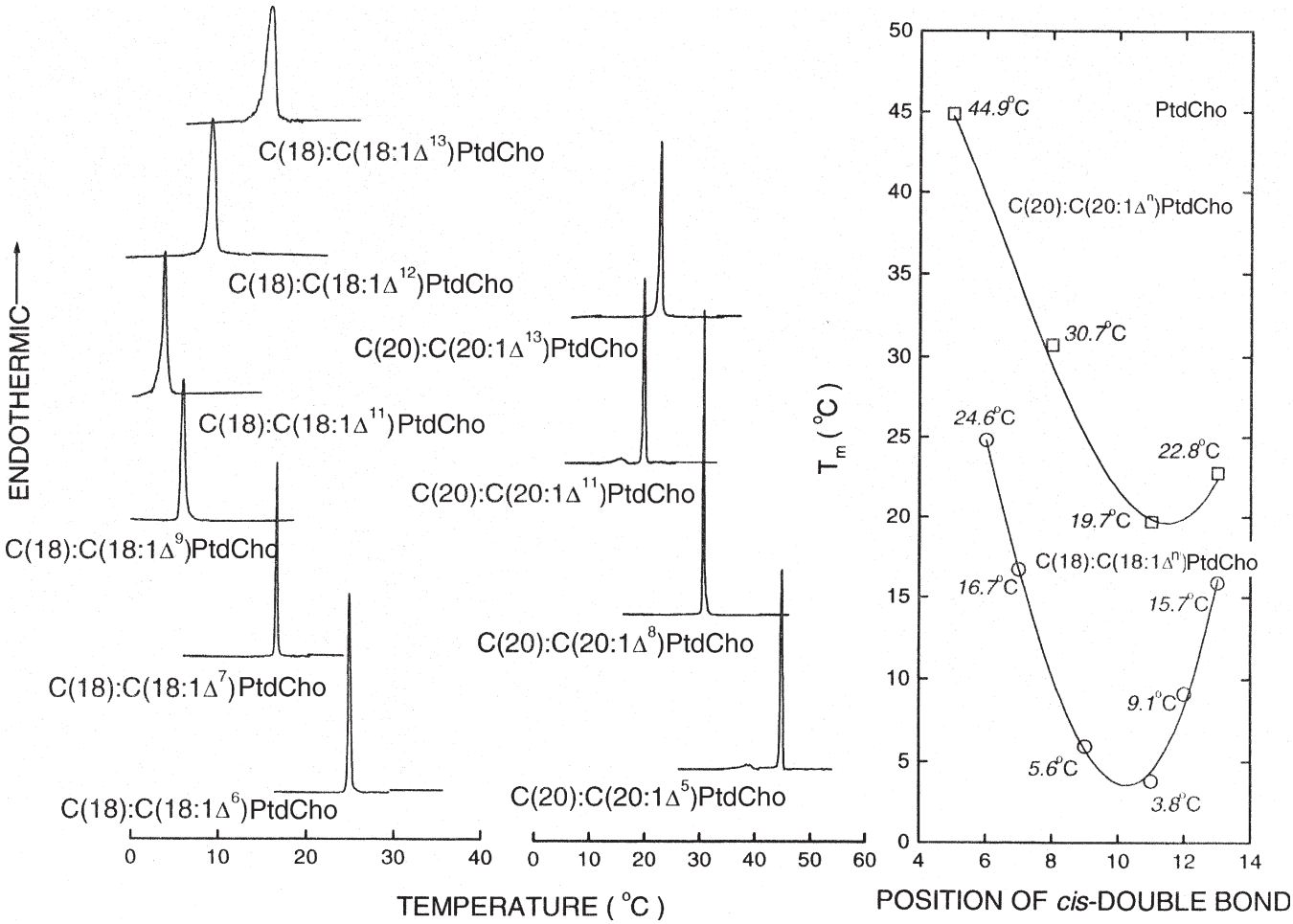

FIG. 9. The T_m-lowering effect of acyl chain monounsaturation as a function of the position of the single *cis*-double bonds. For abbreviation see Figure 3.

lipid molecule with T_m = 3.8°C is calculated to be C(18):C(11)-PtdCho as illustrated in Figure 12. By comparing the energy-minimized structure of the fictive C(18):C(11)PtdCho with that of C(18):C(18:1Δ^{11})PtdCho, one can immediately see that the entire length of the *sn*-2 acyl chain of the fictive molecule is virtually identical to the length of the longer upper chain-segment of the kinked *sn*-2 acyl chain in C(18):C(18:1Δ^{11})PtdCho. At this point, it should be mentioned that the gel-to-liquid crystalline phase transition exhibited by the lipid bilayer at T_m involves fundamentally the rotational *trans* → *gauche* isomerizations of the C–C single bonds in the lipid's acyl chains (24). Based on the energy-minimized structures of the fictive C(18):C(11)PtdCho and C(18):C(18:1Δ^{11})PtdCho shown in Figure 12, we have proposed a molecular model for monounsaturated phospholipids with the following assumptions (13,21): (i) Monounsaturated lipids are assumed to adopt the kinked crankshaft-like motif at $T < T_m$; hence, the kinked *sn*-2 acyl chain consists of a longer chain-segment and a shorter chain-segment at $T < T_m$. (ii) The short chain-segment is assumed to be largely disordered in the gel-state bilayer due to the presence of appreciable *gauche* bonds at $T \leq T_m$. As a result, this short chain-segment does not contribute significantly to the rotationally disordering process of the *trans* → *gauche* isomerizations of the C–C bonds at T_m (3). (iii) The longer chain-segment in the *sn*-2 acyl chain, at $T < T_m$, is assumed to be composed of *trans* rotamers only and to undergo favorable van der Waals contact interactions with its neighboring all-*trans sn*-1 acyl chains in the gel-state bilayer. Hence, the longer chain-segment in the kinked *sn*-2 acyl chain contributes significantly to the thermally induced chain-melting process at T_m.

With the molecular model described above, the drastic T_m-lowering effect of acyl chain monounsaturation can be interpreted. Because the short chain-segment is already disordered at $T < T_m$, the total number of *trans* → *gauche* isomerizations of the C–C bonds at T_m is reduced appreciably for a monounsaturated lipid molecule relative to that of the saturated counterpart, leading to a significantly lower T_m value. We can apply the molecular model to predict the V-shaped T_m profile in the plot of T_m vs. the position of the single *cis*-double bond in the *sn*-2 acyl chain. In this molecular model, the longer chain-segment of the kinked *sn*-2 acyl chain is assumed to undergo favorable van der Waals interactions with its neighboring all-*trans sn*-1 acyl chains. The magnitude of this contact interaction depends on the length of the longer chain-segment. When the Δ-bond is positioned at the center of the *sn*-2 acyl chain, the longer chain-segment has a minimal length,

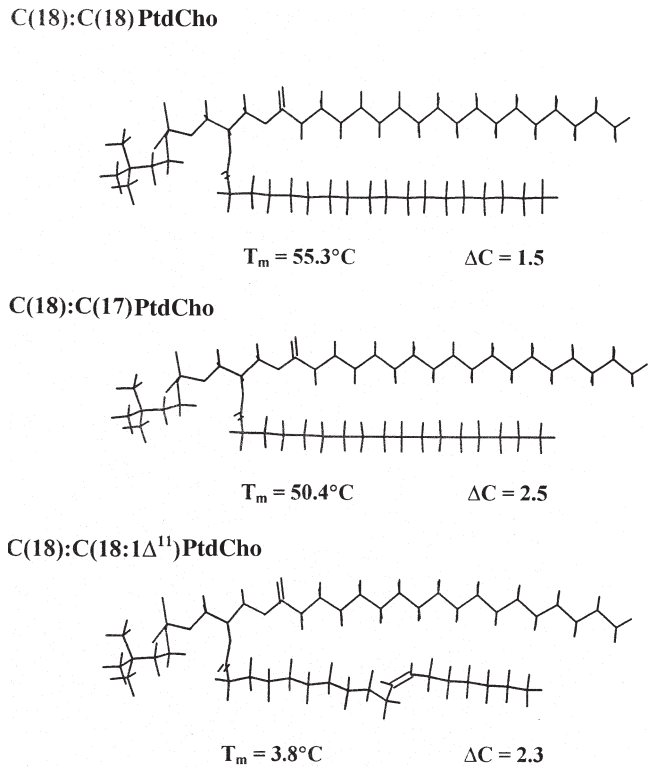

FIG. 10. Computer-graphic representations of the energy-minimized structures obtained with the monomers of C(18):C(18)PtdCho, C(18):C(17)PtdCho, and C(18):C(18:1Δ^{11})PtdCho. For abbreviations see Figure 1.

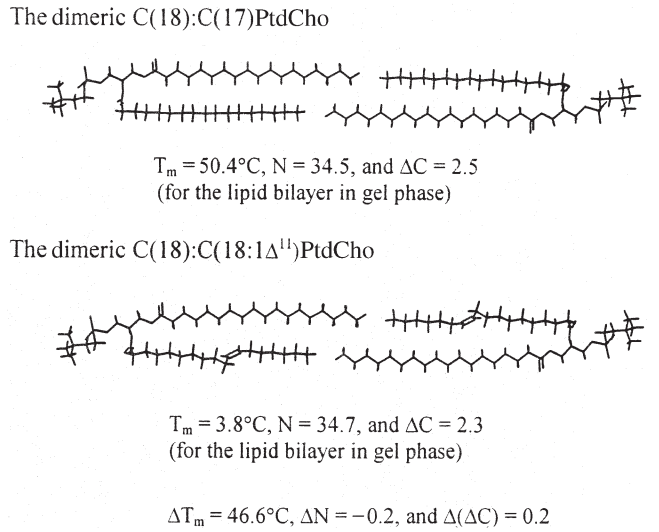

FIG. 11. Computer-graphic representations of the energy-minimized structures obtained with the *trans*-dimers of C(18):C(17)PtdCho and C(18):C(18:1Δ^{11})PtdCho. For abbreviation see Figure 1.

which is almost equal to that of the shorter chain-segment. Consequently, the contact interaction with the all-*trans sn*-1 acyl chain is also minimal. As the Δ-bond moves away stepwise from the chain center toward either end, the length of the longer chain-segment is progressively increased, leading to a proportionally increased van der Waals contact interaction with the all-*trans sn*-1 acyl chain. Because the origin of T_m for the gel-to-liquid crystalline phase transition is largely enthalpic, the T_m can be approximately related to the lateral

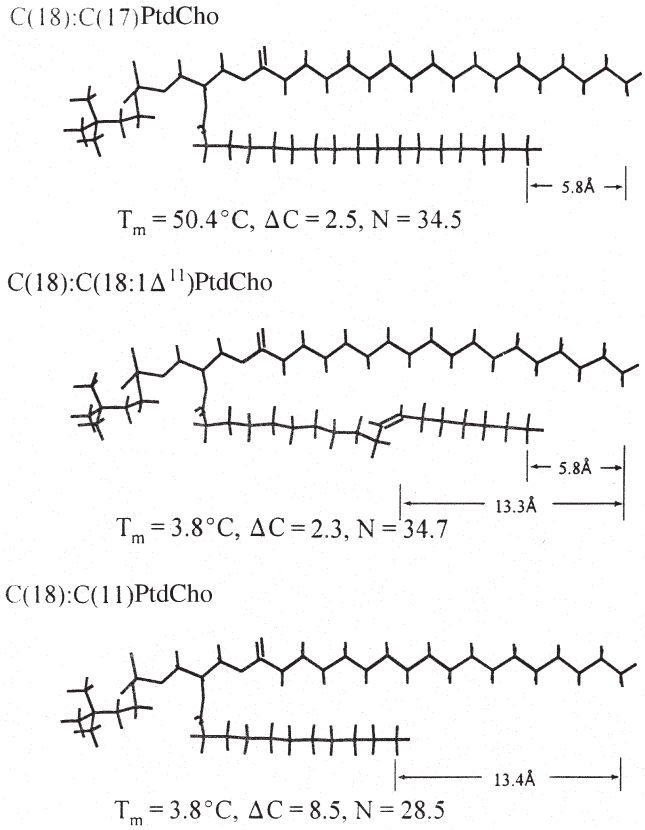

FIG. 12. The structure of the saturated fictive PtdCho molecule calculated on the basis of the T_m and X values of C(18):C(18:1Δ^{11})PtdCho. For abbreviation see Figure 1.

chain-chain contact interaction (13). As a result, the T_m increases as the magnitude of the contact interaction between the *sn*-1 acyl chain and the *sn*-2 acyl chain is increased. Our molecular model thus predicts a V-shaped T_m-profile in the plot of T_m vs. the position of the single *cis*-double bond in the *sn*-2 acyl chain, Δ^n, of mixed-chain C(X):C(Y:1Δ^n)PtdCho. Furthermore, the minimal T_m in the V-shaped T_m-profile must correspond to the positional isomer of C(X):C(Y:1Δ^n)PtdCho with the Δ-bond positioned at the chain center, because the lateral chain-chain interaction is minimal in this lipid species. Indeed, the T_m-profiles observed for the two series of monounsaturated C(18:1Δ^n):C(18:1Δ^n)PtdCho and C(20):C(20:1Δ^n)PtdCho are V-shaped (Fig. 9); in addition, each V-shaped profile is characterized by a minimal T_m corresponding to the anticipated positional isomer.

THE STRUCTURE AND THE CHAIN-MELTING BEHAVIOR OF PHOSPHOLIPIDS WITH *sn*-1 SATURATED AND *sn*-2 POLYUNSATURATED ACYL CHAINS

As discussed above, the presence of just a single *cis*-double bond in the *sn*-2 acyl chain of a phospholipid molecule is sufficient to exert profound influence on the chain-melting behavior of the lipid bilayer. Now, we shall see how the successive addition of a second, a third, . . . methylene-interrupted *cis*-double bond changes the gel-to-liquid crystalline phase

transition behavior of the lipid bilayer. Specifically, I shall present calorimetric data obtained with mixed-chain PtdEth with saturated *sn*-1 and polyunsaturated *sn*-2 acyl chains, since these lipid molecules are present abundantly in biological membranes of animal cells. Moreover, based on the simple molecular model described earlier for monounsaturated lipids, a more general MM-based molecular model will be described, from which the chain-melting behavior of lipid bilayers composed of polyunsaturated mixed-chain lipids can be rationalized in terms of structural changes of the polyunsaturated acyl chain.

The first and the immediate second DSC heating curves obtained with C(20):C(20)PtdEth and its eight unsaturated derivatives are described (Fig. 13). These unsaturated derivatives with two or more *cis*-double bonds in the C_{20}-*sn*-2-acyl chain are seen to contain only methylene-interrupted *cis*-double bonds. The second DSC curves are reproducible upon further repeated reheatings, and the transitions observed in the second heating scans can thus be assigned as the gel-to-liquid crystalline phase transitions. Only the phase transition behavior exhibited by various PtdEth in the second DSC heating scans is discussed in this presentation. For instance, the thermodynamic parameters associated with the gel-to-liquid crystalline phase transition of lipid bilayers prepared from three series of PtdEth are shown in Table 2 (29). More recently, the total numbers of different species of *sn*-1 saturated/*sn*-2 unsaturated PtdEth originated from the common precursors of C(20):C(18)PtdEth and C(20):C(20)PtdEth have been extended in this laboratory to 10 and 15 molecular species, respectively (24,25). In this presentation, I shall limit my discussion of the phase transition behavior of mixed-chain PtdEth to the T_m values of lipid bilayers prepared individually from the 15 lipid species derived commonly from C(20):C(20)PtdEth.

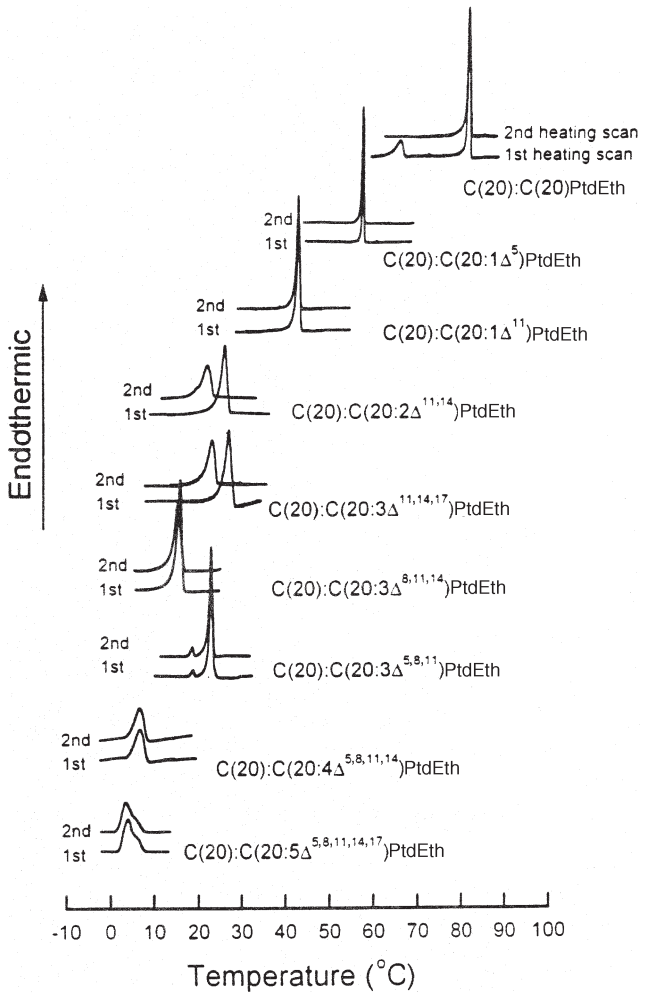

FIG. 13. The first and the immediate second DSC heating curves obtained with C(20):C(20)PtdEth and its eight unsaturated derivatives. Scan rate: 15°C/h. Lipid concentration: ~3–5 mM.

The second DSC heating curves for c(20):C(20)PtdEth and its five unsaturated derivatives of C(20):C(20:1Δ^{17})PtdEth, C(20):C(20:2$\Delta^{14,17}$)PtdEth, C(20):C(20:3$\Delta^{11,14,17}$)PtdEth, C(20):C(20:4$\Delta^{8,11,14,17}$)PtdEth and C(20):C(20:5(^{5,8,11,14,17})-PtdEth are illustrated in Figure 14. Here, the first Δ-bond is incorporated at the n-3 (or Δ^{17})-position in the *sn*-2 acyl chain. The second and all subsequent methylene-interrupted Δ-bonds are introduced into the chain segment located between the n-3-Δ-bond and the carbonyl end. Hence, the *sn*-2 acyl chains of this series of unsaturated PtdEth belong to the n-3-family. In the upper left inset in Figure 14, the T_m value exhibited by each species in the n-3PtdEth series is plotted against the number of Δ-bonds. Clearly, the T_m value decreases continually, but nonlinearly, with increasing number of Δ-bonds. Similarly, like the calorimetric data shown for n-3PtdEth, the T_m value exhibited by each lipid in the unsaturated n-6PtdEth series also decreases

TABLE 2
Thermodynamic Parameters Associated with the Gel-to-Liquid Crystalline Phase Transition of Lipid Bilayers Prepared from Various Phosphatidylethanolamines (PtdEth)

Lipid	T_m (°C)	Δ*H* (kcal/mol)	Δ*S* (cal/mol/K)
C(20):C(20)PtdEth	82.5	12.5	35.2
C(20):C(20:1Δ^{5})PtdEth	58.2	8.3	25.1
C(20):C(20:1Δ^{11})PtdEth	43.3	8.1	25.6
C(20):C(20:2$\Delta^{11,14}$)PtdEth	22.4	4.5	15.2
C(20):C(20:3$\Delta^{11,14,17}$)PtdEth	23.3	6.0	20.2
C(20):C(20:3$\Delta^{8,11,14}$)PtdEth	15.6	5.5	19.1
C(20):C(20:3$\Delta^{5,8,11}$)PtdEth	23.0	5.8	19.6
C(20):C(20:4$\Delta^{5,8,11,14}$)PtdEth	6.6	~5.2	~18.6
C(20):C(20:5$\Delta^{5,8,11,14,17}$)PtdEth	3.5	5.7	20.6
C(20):C(18)PtdEth	75.8	11.2	32.1
C(20):C(18:1Δ^{9})PtdEth	33.9	7.0	22.8
C(20):C(18:2$\Delta^{9,12}$)PtdEth	7.2	3.1	11.1
C(20):C(18:3$\Delta^{9,12,15}$)PtdEth	10.4	4.7	16.6
C(20):C(18:4$\Delta^{6,9,12,15}$)PtdEth	3.9	5.5	19.5
C(18):C(20)PtdEth	79.1	11.5	32.7
C(18):C(20:1Δ^{11})PtdEth	39.5	7.4	23.7
C(18):C(20:2$\Delta^{11,14}$)PtdEth	18.5	3.9	13.4
C(18):C(20:3$\Delta^{11,14,17}$)PtdEth	21.0	5.4	18.4
C(18):C(20:3$\Delta^{8,11,14}$)PtdEth	11.7	5.1	17.9
C(18):C(20:3$\Delta^{5,8,11}$)PtdEth	19.8	5.2	17.8
C(18):C(20:4$\Delta^{5,8,11,14}$)PtdEth	1.3	~4.5	~16.4

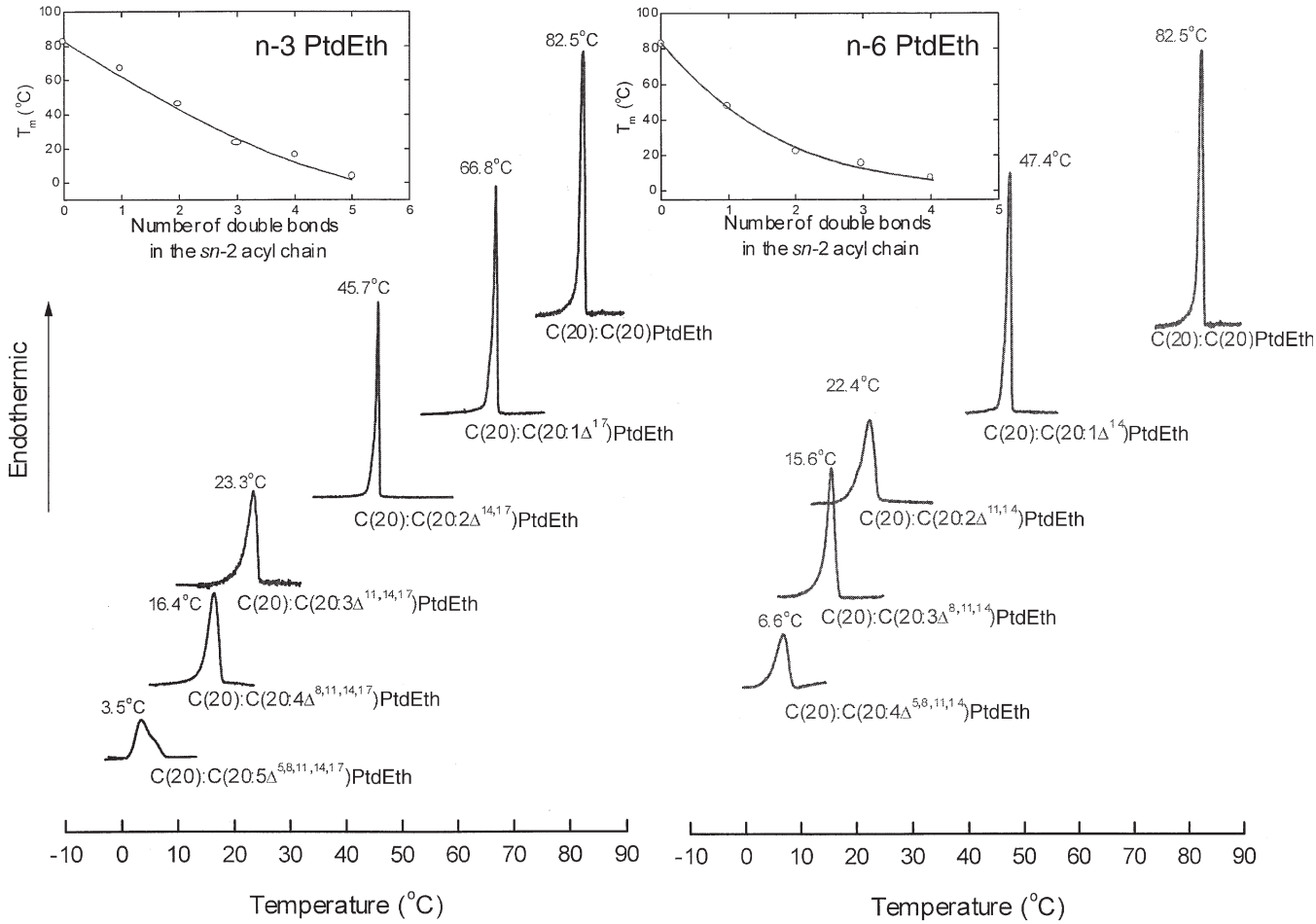

FIG. 14. Representative second DSC heating curves for aqueous dispersions prepared individually from C(20):C(20)PtdEth, five unsaturated n-3 derivatives of C(20):C(20)PtdEth, and four unsaturated n-6 derivatives of C(20):C(20)PtdEth. These unsaturated n-3PtdEth containing n-3 fatty acids and n-6PtdEth containing n-6 fatty acids contain 1–5 and 1–4 *cis*-Δ-bonds, respectively, in the lipid's *sn*-2 acyl chain, with the position of the commonly shared double bond being 3 and 6 carbons from the methyl end, respectively. The abbreviated name for each unsaturated lipid species is indicated under each transition curve, and, above the transition curve, the value of T_m obtained with each lipid dispersion is also indicated. Furthermore, the T_m values obtained with unsaturated lipids in each series are plotted against the number of *cis*-Δ-bonds as shown in the two insets.

continually but nonlinearly with increasing number of Δ-bonds, as shown in the upper right inset in Figure 14. It should be noted that the newly added Δ-bond is also placed on the carbonyl side of the existing Δ-bonds in the n-6PtdEth series.

In Figure 15, the DSC curves exhibited by lipids in two additional series of unsaturated PtdEth are depicted. In these two series of unsaturated PtdEth, the first *cis*-double bonds are introduced into the *sn*-2 acyl chain at the Δ^8- and Δ^{11}-positions, respectively. In contrast to the unsaturated lipids shown in Figure 14, the second and subsequent *cis*-double bonds are always inserted into the *sn*-2 acyl chain at positions located between the existing double bond and the methyl end. Hence, the *sn*-2 acyl chains of these two series of unsaturated PtdEth shown in Figure 15 belong to the Δ^8- and the Δ^{11}-series. For the Δ^{11}PtdEth series, the T_m value of C(20):C(20)PtdEth is seen in Figure 15 to decrease from 82.5 to 43.3°C upon the introduction of the first Δ-bond. A further decrease of 20.9°C in T_m is observed in going from C(20):C(20:1Δ^{11})PtdEth → C(20):C(20:2$\Delta^{11,14}$)PtdEth. In contrast, a slight increase in T_m (0.9°C) is detected as the third methylene-interrupted *cis*-double bond is subsequently added to the dienoic *sn*-2 acyl chain on the methyl end of the Δ^{14}-double bond. Structurally, the C(20):C(20:2$\Delta^{11,14}$)PtdEth → C(20):C(20:3$\Delta^{11,14,17}$)PtdEth conversion, characterized by a small increase in T_m, corresponds to an n-6PtdEth → n-3PtdEth conversion. When all T_m values obtained with lipids in this Δ^{11}-PtdEth series are plotted against the number of *cis*-double bonds, a down-and-up T_m-profile is observed (upper right inset, Fig. 15). Similarly, for lipids in the Δ^8-PtdEth series, the variation of T_m as a function of the number of Δ-bonds is also characterized by a down-and-up trend (upper left inset, Fig. 15). In this case, the lipid with four Δ-bonds, C(20):C(20:4$\Delta^{8,11,14,17}$)PtdEth, is an n-3PtdEth which displays a higher T_m value than its precursor, C(20):C(20:3$\Delta^{8,11,14,}$)-PtdEth, an n-6PtdEth with three Δ-bonds.

Based on the T_m values shown in Figures 14 and 15 and some other DSC data published previously, a T_m diagram is constructed as shown in Figure 16 (25). Here, nine series of mixed-chain PtdEth with saturated C_{20}-*sn*-1 and unsaturated C_{20}-*sn*-2 acyl chains derived from the common precursor of

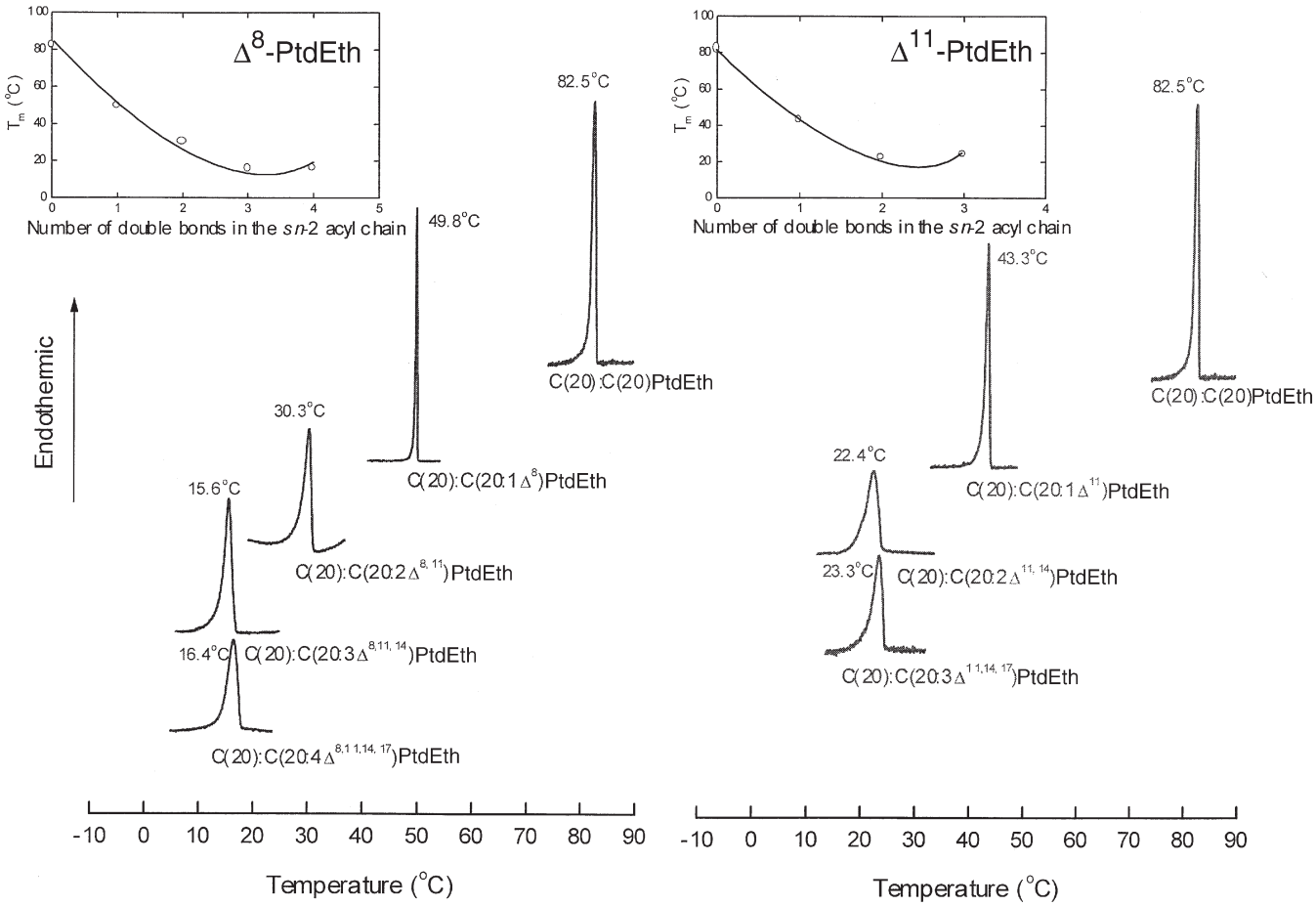

FIG. 15. The second DSC heating curves exhibited by lipids in the Δ^8PtdEth- and Δ^{11}PtdEth-series. Here, the superscript number denotes the position of the common *cis*-double bond in the *sn*-2 acyl chain when counting from the carbonyl end.

saturated C(20):C(20)PtdEth are presented. In each of these nine series of PtdEth, there are three or more lipids that share either a common Δ-bond at a fixed position along the *sn*-2 acyl chain or a fixed number of Δ-bonds. In this T_m diagram, all T_m values are placed underneath the appropriate structural formulas. These formulas are arranged systematically in a unifying manner according to their order of complexity. From Figure 16, the effects of the number and position of Δ-bonds on the T_m obtained with lipids in the nine series of mixed-chain unsaturated C_{20}-PtdEth can thus be examined simply and simultaneously. Let us first look at the 3-series of PtdEth aligned horizontally in Figure 16; mixed-chain lipids in each of the three n-3 to n-9 PtdEth-series are characterized by a continuously decreasing T_m profile as the number of Δ-bonds increases progressively. Similarly, mixed-chain lipids in the Δ^5-PtdEth series aligned vertically along the rightmost line in the T_m-diagram also display a decreasing T_m profile. However, as discussed earlier, the C(20):C(20:2$\Delta^{11,14}$)PtdEth → C(20):C(20:3$\Delta^{11,14,17}$)PtdEth and the C(20):C(20:3$\Delta^{8,11,14}$)-PtdEth → C(20):C(20:4$\Delta^{8,11,14,17}$)PtdEth conversions are coupled with increased values of T_m. For the Δ^8- and Δ^{11}-PtdEth series that are also aligned vertically in Figure 16, the T_m-profiles are characterized by a down-and-up trend. Finally, three series of mixed-chain PtdEth each with a fixed number of Δ-bonds in the *sn*-2 acyl chain can be seen along the diagonal lines in the T_m-diagram (Fig. 16). The monoenoic, dienoic, and trienoic series of mixed-chain PtdEth have five, four, and three positional isomers, respectively. In response to changes in the position of the double bond, the T_m values of mixed-chain lipids with a fixed number of Δ-bonds give rise to a roughly V-shaped profile, a scenario that has been discussed earlier in details for monounsaturated lipids. Interestingly, the two series of positional isomers of PtdEth containing two and three *cis*-double bonds also exhibit V-shaped T_m-profiles in the plot of T_m vs. the position of *cis*-double bonds. The most novel feature of the T_m-diagram shown in Figure 16 is the following: all the different T_m profiles observed for mixed-chain lipids derived from a common precursor of a saturated lipid species can be seen simultaneously in a simple and unifying manner.

The energy-minimized structures of monounsaturated mixed-chain PtdCho such as C(16):C(18:1Δ^9)PtdCho obtained with MM calculations have been presented. Similar structures can also be simulated for monounsaturated mixed-chain PtdEth based on the single-crystal data of PtdEth (26) and the atomic coordinates of the energy-minimized structures of monoenoic hydrocarbons (22). For instance, a kinked crankshaft-like structure with low energy is simulated for

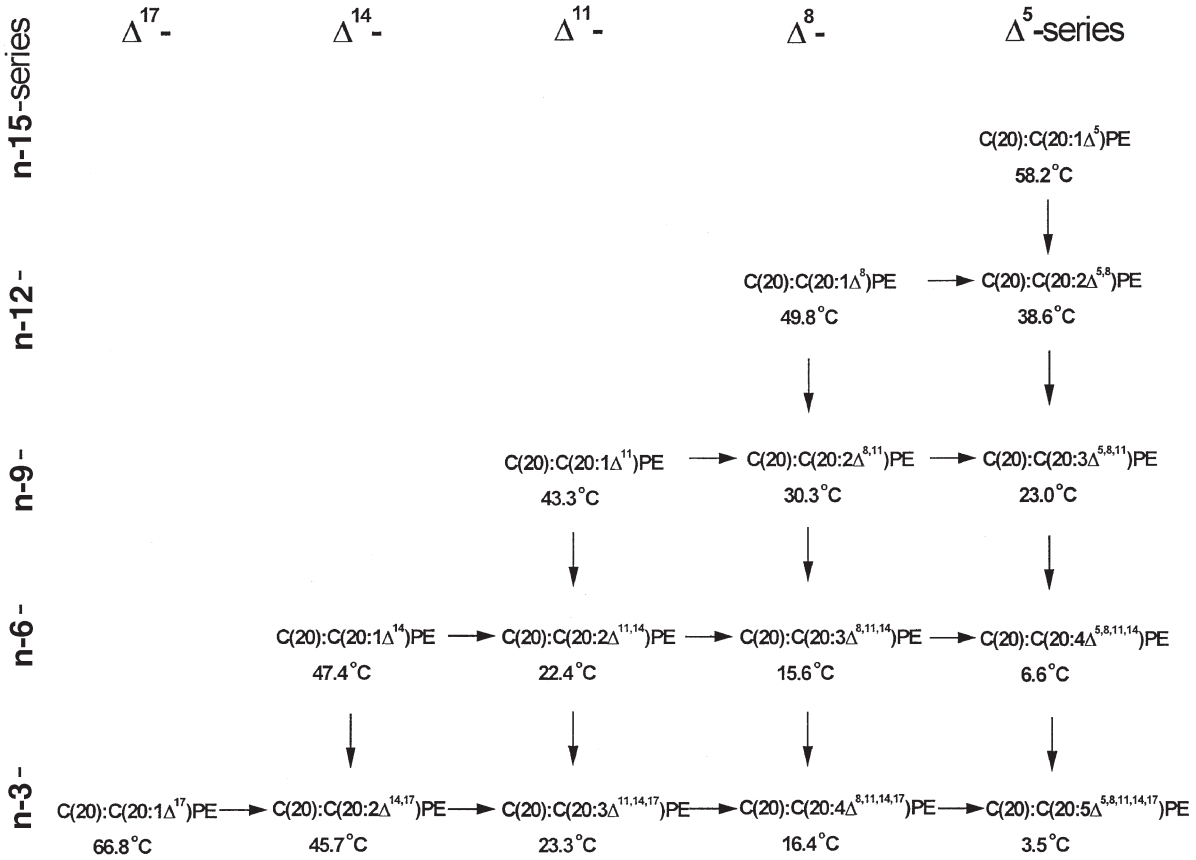

FIG. 16. The T_m-diagram of *sn*-1 C_{20}-saturated/*sn*-2 C_{20}-unsaturated PtdEth. Lipids in each row share a common n-carbon, where the n-carbon is defined as the first olefinic carbon atom in the lipid's *sn*-2 acyl chain when counting from the chain terminal methyl end. The five parallel rows of unsaturated lipids from top to bottom are n-15PtdEth, n-12PtdEth, n-9PtdEth, n-6PtdEth, and n-3PtdEth series as indicated. Lipids in each column share a common Δ^n-bond, and lipids in each column thus belong to a Δ^nPtdEth series, where the superscript *n* denotes the position of the common *cis* carbon-carbon double bond in the *sn*-2 acyl chain when counting from the carbonyl end. In this case, the carbonyl carbon is designated as the first carbon of the acyl chain. The five columns of unsaturated lipids from left to right are Δ^{17}PtdEth, Δ^{14}PtdEth, Δ^{11}PtdEth, Δ^8PtdEth, and Δ^5PtdEth series, respectively, as indicated. Altogether, there are 15 molecular species of unsaturated mixed-chain PtdEth in this T_m diagram, and their T_m values are given under the abbreviated names of the corresponding mixed-chain PtdEth.

C(16):C(18:1Δ^9)PtdEth (Fig. 17). Furthermore, the single-crystal structure of linoleic acid, determined by Ernst *et al.* (27), is characterized by a crankshaft-like motif with a kink sequence of $s^-\Delta s^+s^+\Delta s^-$ (–119, –2.3, 123, 124, –3.3, –121°). The most stable structure of dienoic PtdEth in the crystalline-state bilayer can thus be expected to have a kinked conformation. As expected, a rotamer with a kink sequence of $s^-\Delta s^+s^+\Delta s^-$ is indeed found by MM calculations to be energetically the most stable conformation for the s*n*-2 acyl chain of C(16):C(18:2$\Delta^{9,12}$)PtdEth (Fig. 17; 28). MM simulations, in fact, further show that the roughly crankshaft-like conformation is a common motif underlying the energy-minimized structure of other *sn*-2 acyl chains of mixed-chain PtdEth containing three or more methylene-interrupted Δ-bonds (Fig. 18).

The energy-minimized structures of C(20):C(20)PtdEth and its five unsaturated n-3 derivatives are illustrated in Figure 19 (25). These structures, to a first approximation, correspond to the optimal and static structures of PtdEth molecules packed in the crystalline-state bilayer. Here, the zigzag plane of the all-*trans* *sn*-1 acyl chain in each lipid species lies perpendicular to the paper plane, whereas the *sn*-2 acyl chain projects in front of the *sn*-1 acyl chain. For C(20):C(20)-PtdEth, the *sn*-2 acyl chain has an all-*trans* segment extending from C(3) to C(19) with 17 methylene units. This segment is designated as the all-*trans* segment, abbreviated as ATS. For C(20):C(20:1Δ^{17})PtdEth, the *sn*-2 acyl chain has a crankshaft-like topology with a kink sequence given under the energy-minimized structure in Figure 19. As a result, the *sn*-2 acyl chain can be viewed to consist of two chain segments linked by the kink sequence. The all-*trans* segment in the long-chain segment of the kinked *sn*-2 acyl chain is defined as the ATS. For C(20):C(20:1Δ^{17})PtdEth, the ATS has 14 consecutive methylene units extending from C(3) to C(16) along the kinked *sn*-2 acyl chain. Note that the ATS is one C–C bond length shorter than that of the long chain segment due to the fact that the C–C single bond preceding the Δ^{17}-bond has an s^- conformation. For the energy-minimized structures of polyunsaturated n-3PtdEth shown in Figure 19, the *sn*-2 acyl chains are seen to adopt roughly an overall kinked motif. The ATS is observed invariably to locate in the upper chain segment in each kinked *sn*-2 acyl chain. Moreover, the length of the ATS is shortened progressively by three methylene

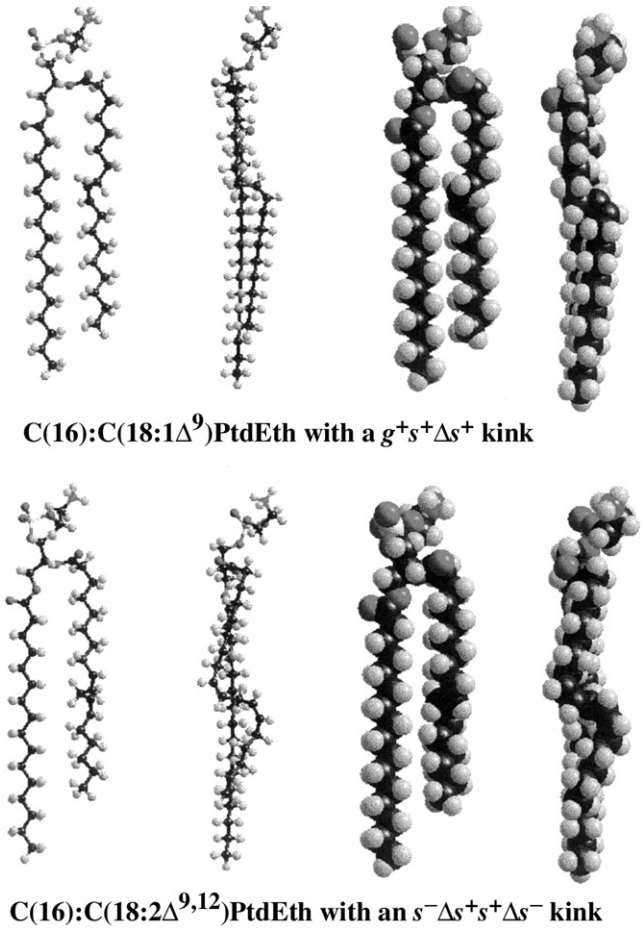

FIG. 17. The energy-minimized structures of C(16):C(18:1Δ^{9})PtdEth and C(16):C(18:2$\Delta^{9,12}$)PtdEth; each is characterized by a kinked crankshaft-like motif.

units as a Δ-bond is added successively on the carbonyl side of the existing Δ-bonds at the methylene-interrupted position. In contrast, the short chain segment succeeding the Δ^{17}-bond is identical in length (Fig. 19). It should be emphasized that the structural features of polyunsaturated n-3PtdEth mentioned above are simulated results obtained with MM computations. These simulated structures do not explicitly provide information about the dynamic nature of lipid molecules in the gel-state bilayer. For instance, the *sn*-2 acyl chains of all unsaturated n-3PtdEth shown in Figure 19 share a common chain terminal segment of C(16)-C(17)=C(18)-C(19)-C(20), in which all C–C single bonds are most likely dynamic in the gel-state bilayer. The assumed flexible nature at $T < T_m$ can be attributed mainly to the large degree of rotational freedom of two single C–C bonds adjacent to the Δ-bond as well as the C–C single bond containing the methyl terminal carbon atom. Hence, it is reasonable to suppose that this disordered methyl terminal segment does not undergo the thermally induced *trans* → *gauche* isomerizations at T_m, and it thus makes no contributions to the chain disordering process at T_m. The dynamic nature of this short terminal segment, however, is not revealed by any of the MM simulated structures illustrated in Figure 19. On the other hand, as the number of Δ-bonds in this series of n-3PtdEth increases from zero to five, the length of ATS is shortened in each step by a constant length of three methylene units. This variation in ATS, shown clearly in Figure 19, is considered to be a structural feature that persists in the gel-state bilayer.

Similar to lipids in the n-3PtdEth series, the five lipids in the Δ^{5}PtdEth series seen in the T_m diagram also contain up to five methylene-interrupted Δ-bonds in the *sn*-2 acyl chain. The energy-minimized structures of these lipids have also been determined by MM calculations, and a crankshaft-like topology characterizes them all. In these lipids, the short chain segments in the kinked *sn*-2 chains are located near the H_2O/hydrocarbon interface, extending from C(3) to C(5). All ATS, however, are located in the lower chain segments; the length of each ATS decreases progressively by three methylene units as a methylene-interrupted Δ-bond is added successively on the methyl side of the existing Δ-bond(s). This decreasing trend in ATS is, in essence, identical to that observed in Figure 19 for the n-3PtdEth series.

In Figure 20, the minimum-energy structures of C(20):C(20:1Δ^{11})PtdEth, C(20):C(20:2$\Delta^{11,14}$)PtdEth, and C(20):C(20:3$\Delta^{11,14,17}$)PtdEth in the Δ^{11}PtdEth series are illustrated. For C(20):C(20:1Δ^{11})PtdEth, the Δ^{11}-double bond is located in the middle of the *sn*-2 acyl chain, and the additional Δ-bonds in C(20):C(20:2$\Delta^{11,14}$)PtdEth and (20):C(20:3$\Delta^{11,14,17}$)PtdEth are on the methyl side of the Δ^{11}-bond. Unlike the variable length of ATS shown in Figure 19, all three lipids in this series of Δ^{11}PtdEth share a constant chain length of ATS extending from C(3) to C(10) in the *sn*-2 acyl chain (Fig. 20). It is evident that as the C(20):C(20:2$\Delta^{11,14}$)-PtdEth (an n-6PtdEth) → C(20):C(20:3$\Delta^{11,14,17}$)PtdEth (an n-3PtdEth) conversion occurs, the added Δ^{17}-bond is introduced on the methyl side of the existing Δ-bonds, and the length of the ATS is not affected by the n-6PtdEth → n-3PtdEth conversion. The last two Δ^{8}PtdEth species shown in the T_m-diagram are C(20):C(20:3$\Delta^{8,11,14}$)PtdEth and C(20):C(20:4$\Delta^{8,11,14,17}$)-PtdEth, which are n-6PtdEth and n-3PtdEth, respectively. Interestingly, they share a constant length of ATS that is located in the upper chain segment of the kinked *sn*-2 acyl (25). The fourth Δ-bond is added on the methyl side of the existing Δ-bonds as the n-6PtdEth → n-3PtdEth conversion takes place. Hence, this n-6PtdEth → n-3PtdEth conversion is structurally similar to the C(20):C(20:2$\Delta^{11,14}$)PtdEth (an n-6PtdEth) → C(20):C(20:3$\Delta^{11,14,17}$)PtdEth (an n-3PtdEth) conversion seen in Figure 20.

Let me summarize what is known about the structural features of *sn*-1 saturated/*sn*-2 polyunsaturated phospholipids from MM simulations: (i) the *sn*-1 acyl chain has an all-*trans* conformation; (ii) the *sn*-2 acyl chain extending from C(3) to the methyl terminus has a crankshaft-like conformation; hence, it can be considered to consist of two chain-segments linked by a kink sequence; (iii) the relative length of the two chain-segments in the kinked *sn*-2 acyl chain depends on the position of the multiple Δ-bonds; (iv) the consecutive all-*trans* segment in the long chain segment of the kinked *sn*-2 chain can be defined as ATS, and the length of ATS is

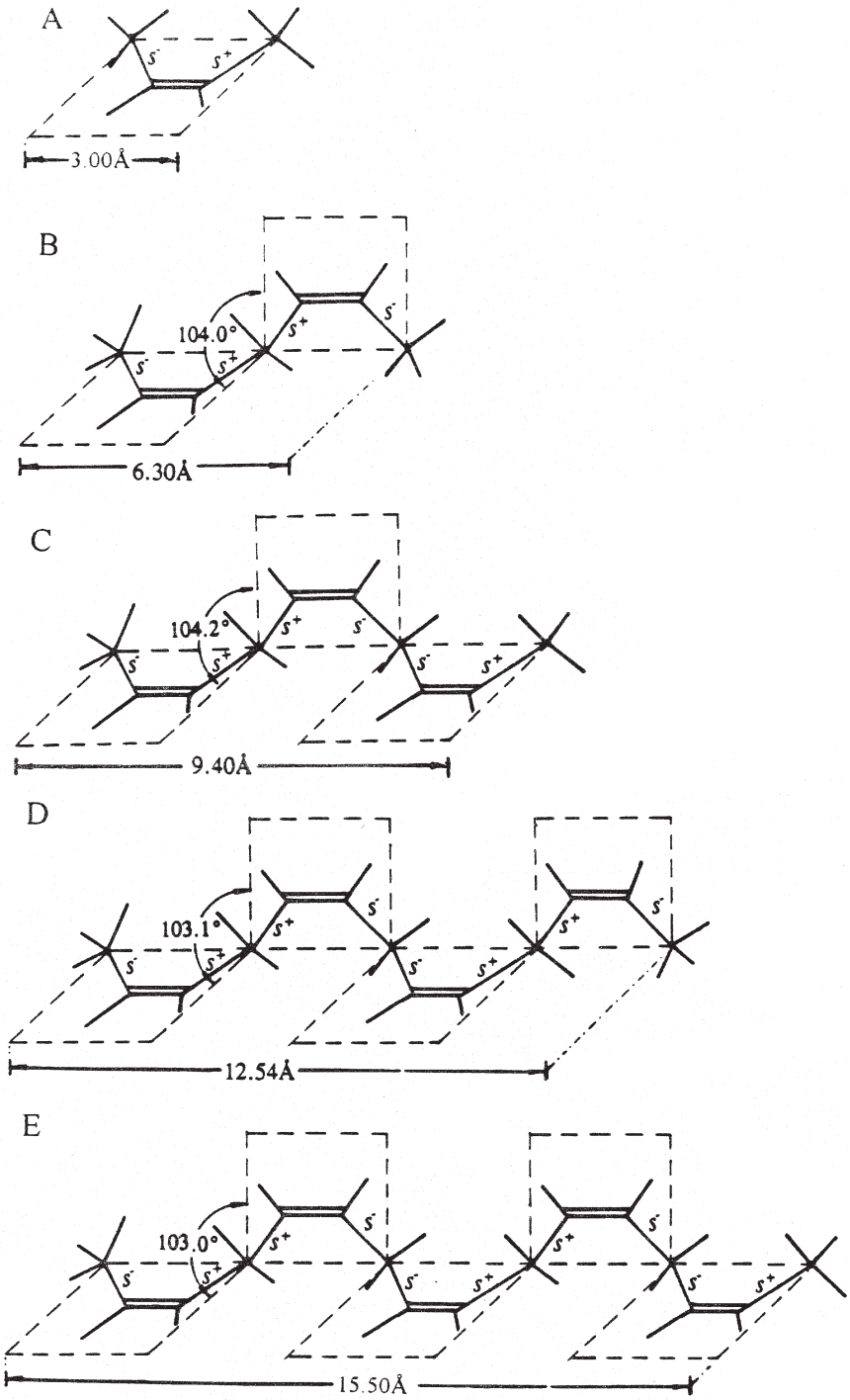

FIG. 18. The energy-minimized structure of hydrocarbon chains containing 1–5 methylene-interrupted *cis*-double bonds.

shortened by three methylene units if a methylene-interrupted Δ-bond is incorporated into the ATS; (v) the kink sequence in the dienoic *sn*-2 acyl chain is $s^{-}\Delta s^{+}s^{+}\Delta s^{-}$ or $s^{+}\Delta s^{-}s^{-}\Delta s^{+}$, depending on whether the position of *n* in $\Delta^{n,n+3}$-bond is an odd- or even-carbon atom in the *sn*-2 acyl chain.

Earlier, we presented a simple molecular model that can interpret adequately the large T_m-lowering effect of acyl chain monounsaturation and the V-shaped characteristic dependency of T_m on the position of the single Δ-bond along the *sn*-2 acyl chain. We can extend this simple model to interpret the different effects of the *sn*-2 acyl chain polyunsaturation on the phase transition behavior as seen in the T_m-diagram (Fig. 16). In this extended molecular model, three basic assumptions are made. (i) The *sn*-2 acyl chain in the mixed-chain PtdEth (or PtdCho) with *sn*-1 saturated/*sn*-2 unsaturated acyl chains is assumed to adopt, at $T < T_m$, an energy-minimized crankshaft-like kink motif. Hence, it consists of a longer and a shorter chain-segment separated by the Δ-containing kink. (ii) At $T < T_m$, the

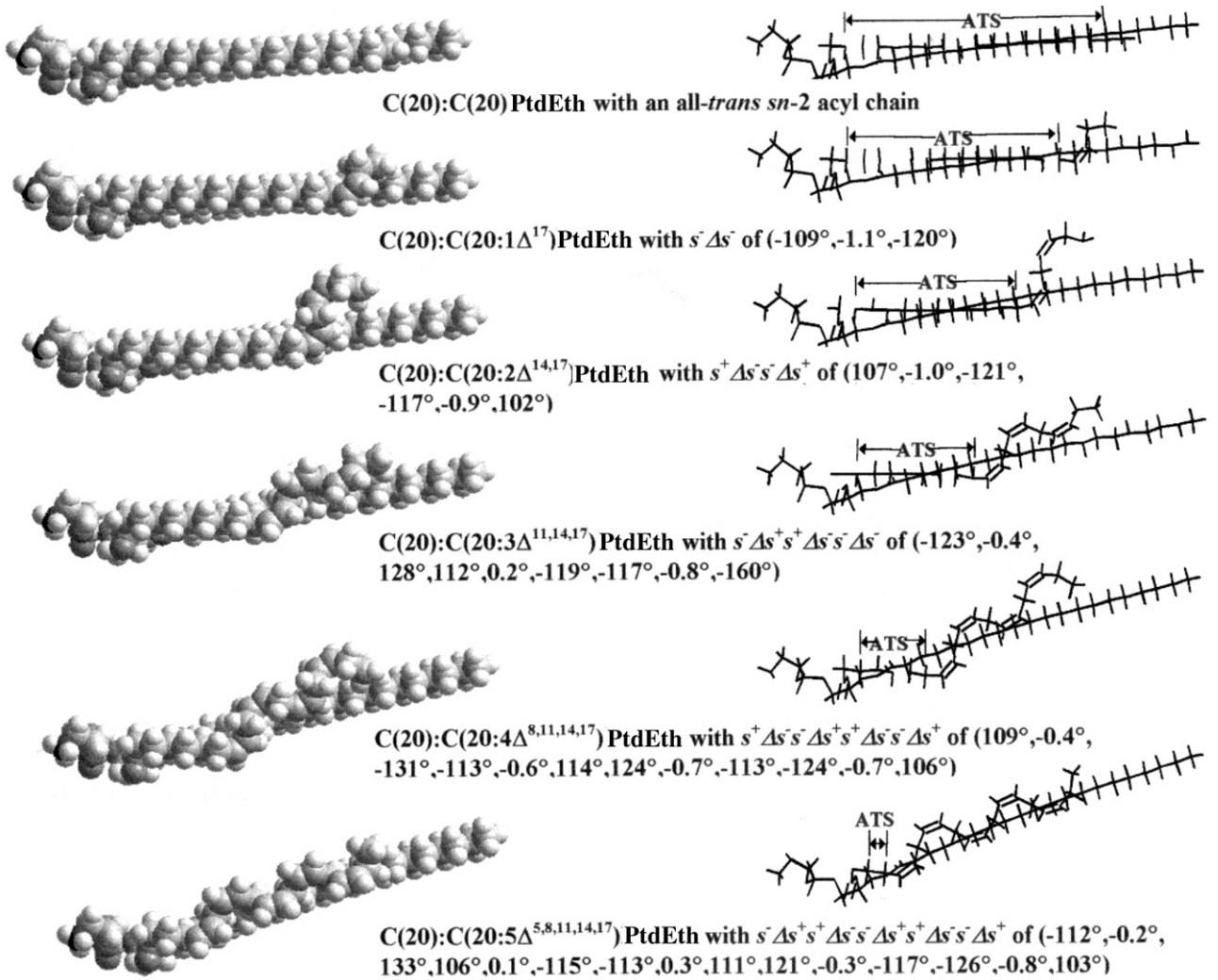

FIG. 19. The energy-minimized structures of C(20):C(20)PtdEth and its five unsaturated n-3 derivatives as shown molecular-graphically by space-filling and wire models. These unsaturated n-3PtdEth molecules contain 1–5 *cis*-Δ-bonds. The ATS shown in the wire model denotes the all-*trans* segment (ATS) of the hydrocarbon chain in the *sn*-2 acyl chain. The kink sequence in the *sn*-2 unsaturated acyl chain and a set of optimal torsion angles associated with the kink sequence are presented under each unsaturated lipid species. The length of ATS is shortened progressively by three methylene units as the new methylene-interrupted *cis*-double bond is added successively on the carbonyl side of the Δ^{17}-bond in the *sn*-2 acyl chain of C(20):C(20:1Δ^{17})PtdEth. In contrast, the short chain segment succeeding the Δ^{17}-bond is identical in length.

ATS in the long chain segment of the kinked *sn*-2 acyl chain and the neighboring all-*trans sn*-1 acyl chain are proposed to undergo attractive van der Waals interaction. In contrast, the shorter chain-segment of the kinked *sn*-2 acyl chain is assumed to be partially disordered. However, if the length of the shorter chain-segment differs from that of the longer one by 1–3 C–C bond lengths, the shorter chain-segment may contribute somewhat to the chain-melting process at T_m. (iii) When the number of Δ-bonds in the *sn*-2 acyl chain is larger than two, the methylene-interrupted Δ-bonds act together as a rigid structural unit, which prevents the rotational isomerizations of C–C bonds in the neighboring chains. Hence, the *sn*-2 acyl chain with three or more methylene-interrupted Δ-bonds can facilitate somewhat the lateral chain-chain interactions in the gel-state bilayer.

According to the extended molecular model presented above, the variations of T_m upon successive chain unsaturation in the *sn*-2 acyl chain reflect mainly the changes of the following two opposing effects: (i) the T_m-lowering effect caused by the progressive shortening of ATS, and (ii) the T_m-elevating effect exerted by the increased rigidity of three to five Δ-bonds. These two opposing effects are brought about, paradoxically, by the same structural change, by the increasing degree of acyl chain unsaturation in the *sn*-2 position. We can now apply this model to explain why two distinct types of T_m profile are observed for lipids upon the successive addition of methylene-interrupted Δ-bonds in the *sn*-2 acyl chain. One type is characterized by a nonlinearly decreased T_m-curve and the other is characterized by a down-and-up T_m-profile in the plot of T_m vs. the number of Δ-bonds in the *sn*-2 acyl chain.

We begin with the discussion of the T_m profile exhibited by lipids in the n-3PtdEth series derived from C(20):C(20)-PtdEth. This series can be taken as an example to represent all series of PtdEth characterized by a nonlinearly decreased T_m profile. As shown in Figure 21, the length of ATS is short-

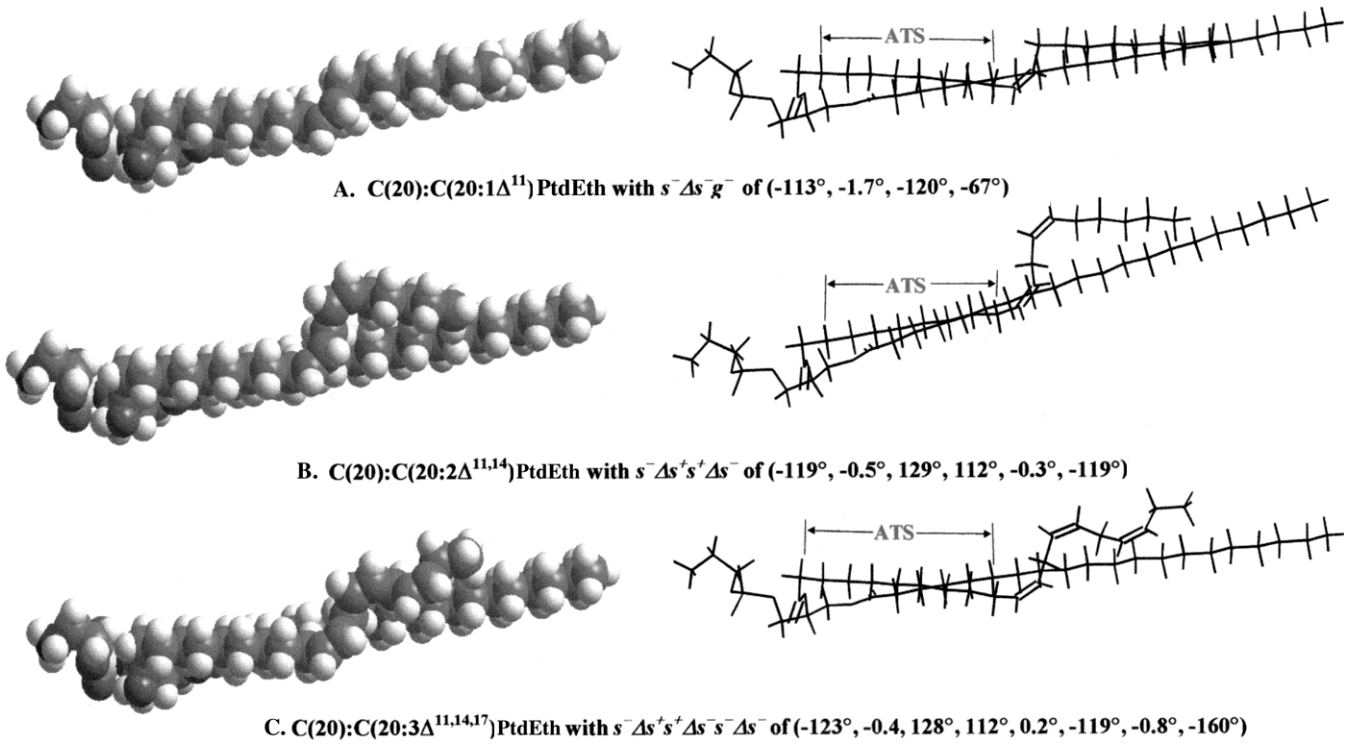

FIG. 20. Molecular graphics representations of the energy-minimized structures of C(20):C(20:1Δ^{11})PtdEth, C(20):C(20:2$\Delta^{11,14}$)PtdEth, and C(20):C(20:3$\Delta^{11,14,17}$)PtdEth in the Δ^{11}PtdEth series as depicted by ball-and-stick and space-filling models. ATS in each lipid species is located in the upper chain-segment of the kinked *sn*-2 acyl chain; moreover, a constant length of ATS is shared by all three lipid species. The added Δ-bond is introduced on the methyl side of the existing Δ-bond. The kink sequence and associated torsion angles for each unsaturated acyl chain are presented under the energy-minimized structure of the corresponding lipid. For abbreviations see Figures 1 and 19.

ened progressively by a constant length of three methylene units as a methylene-interrupted Δ-bond is added successively into the *sn*-2 acyl chain. Based on the observed constant decrease in ATS alone, the T_m values of lipids in the n-3PtdEth series can be expected to fall on a straight line with a negative slope. On the other hand, when the total number of Δ-bonds in the *sn*-2 acyl chain is three or more, the multiple Δ-bonds are proposed to act as a rigid structural unit, thus leading to a gradual increase in T_m. However, we assume that this T_m-elevating effect is less than the T_m-lowering effect exerted by the shortening of the ATS in the *sn*-2 acyl chain. On balance, the absolute value of the T_m increment will be decreased progressively as the third and subsequent Δ-bonds are introduced stepwise into the *sn*-2 acyl chain, with the largest decrease in the T_m increment occurring at the highest number of Δ-bonds. Consequently, the T_m values of lipids in the n-3PtdEth series in the plot of T_m vs. the number of Δ-bonds are expected to fall on a nonlinearly decreased curve; furthermore, the T_m from the lipid species with the highest number of Δ-bonds is expected to deviate most from the straight line. These expectations are indeed borne out by experimental data (Fig. 21). Therefore, we may conclude that the presence of *cis*-double bonds in the *sn*-2 acyl chain contributes to the positive deviation of T_m from the linear T_m-profile in the plot of T_m vs. the number of *cis*-double bonds, although its effect vanishes when the total number of Δ-bonds in the *sn*-2 acyl chain is equal to or less than two.

Our proposed model can also explain the down-and-up T_m-profile exhibited by lipids in the Δ^8PtdEth- and Δ^{11}PtdEth-series shown in the T_m diagram. Here, the Δ^{11}PtdEth-series is chosen as an example to illustrate our points. The energy-minimized structures of the three lipid species in the Δ^{11}PtdEth-series are shown in Figure 22, in which the ATS is seen to locate in the upper chain-segment. Moreover, the length of ATS remains unchanged among the three lipid species. It should be noted that the lower chain-segment in the C(20):C(20:1Δ^{11})PtdEth has a length that is only one C–C bond length shorter than the upper chain-segment. According to our proposed molecular model, this short chain-segment may contribute somewhat to the chain-melting process at T_m. Consequently, the T_m value for the lipid bilayer composed of C(20):C(20:1Δ^{11})PtdEth can be expected to be higher than that of C(20):C20:2$\Delta^{11,14}$)PtdEth, although these two unsaturated lipids share a common length of ATS. The introduction of a third *cis*-double bond into the *sn*-2 acyl chain of C(20):C(20:2$\Delta^{11,14}$)PtdEth, an n-6PtdEth, converts the lipid into an n-3PtdEth, or C(20):C(20:3$\Delta^{11,14,17}$)-PtdEth. Based on the constant length of ATS alone, the T_m increment between the n-6PtdEth and the n-3PtdEth would be zero. However, the n-3PtdEth has an additional Δ-bond in comparison to the n-6PtdEth; based on our proposed molecular model, a positive T_m increment is thus expected to associate with the n-6PtdEth → n-3PtdEth conversion in this Δ^{11}PtdEth series. On the basis of our proposed molecular

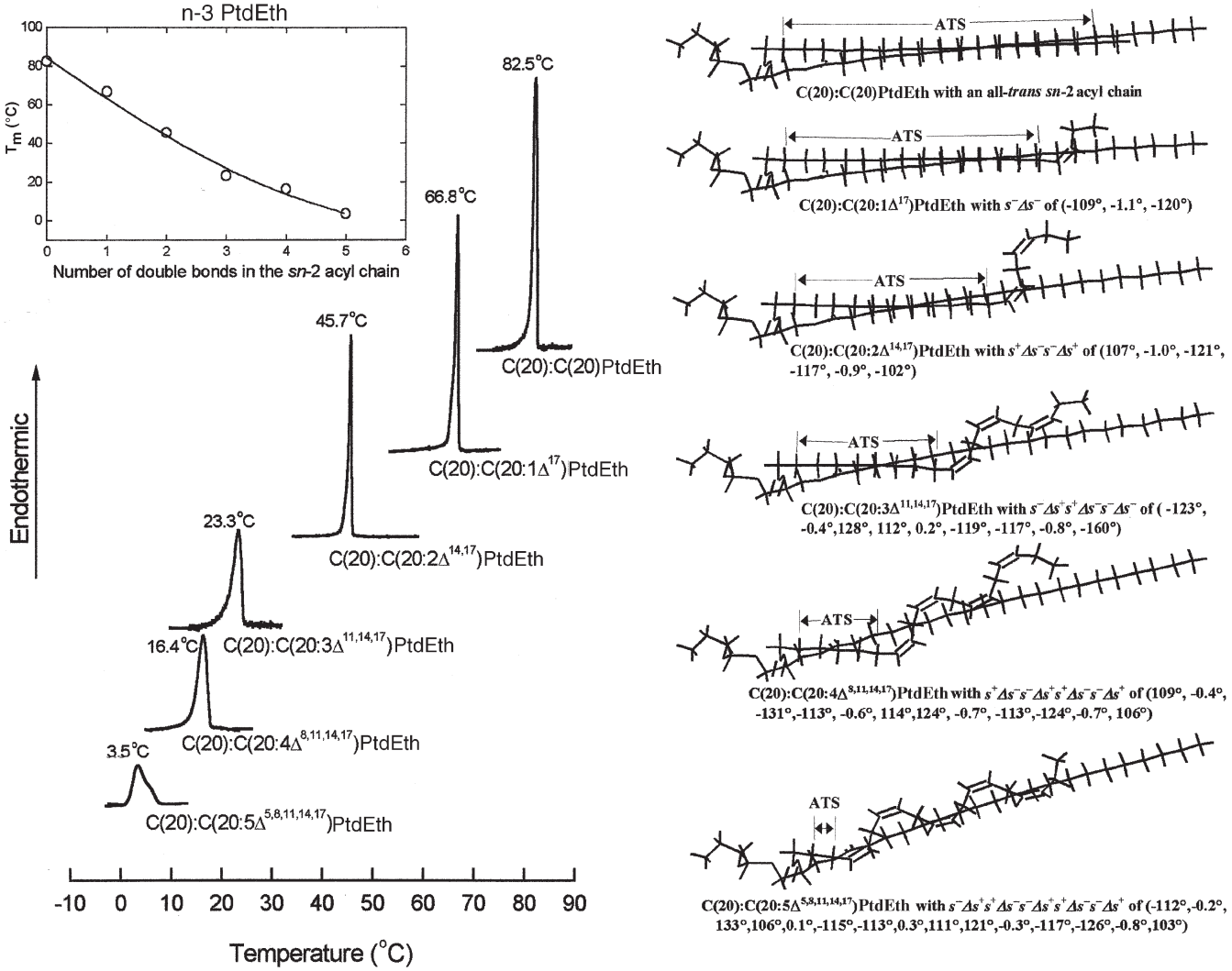

FIG. 21. The energy-minimized structures of C(20):C(20)PtdEth and its five unsaturated n-3 derivatives are presented in the presence of the thermograms exhibited by these six lipid species. The T_m-profile shown in the inset can be roughly correlated with the variation of the ATS length in the *sn*-2 acyl chains of these six lipid species.

model, the consecutive C(20):C(20:1Δ^{11})PtdEth $\rightarrow$ C(20):C(20:2$\Delta^{11,14}$)PtdEth $\rightarrow$ C(20):C(20:3$\Delta^{11,14,17}$)-PtdEth conversion should be accompanied by a down-and-up T_m-profile. And this is indeed observed calorimetrically as shown in Figure 22. Moreover, such a down-and-up T_m-profile has also been observed calorimetrically for PtdCho in two different Δ^{11}PtdCho series (29).

I would now like to conclude by considering once more the T_m-diagram (Fig. 16) constructed for mixed-chain phospholipids with saturated and unsaturated *sn*-1 and *sn*-2 acyl chains, respectively, that are originated from a common precursor, C(20):C(20)PtdEth. All unsaturated lipids with two or more *cis*-double bonds shown in this T_m-diagram have methylene-interrupted *cis*-double bonds, which are the hallmark of the naturally occurring phospholipids found in animal cells. Moreover, the energy-minimized structures of all the unsaturated *sn*-2 acyl chains of lipids shown in this T_m-diagram are characterized by a kinked crankshaft-like motif as obtained by MM calculations. A novel virtue of this T_m-diagram is that the T_m-profiles exhibited by various series of lipids arranged along the horizontal, vertical, and diagonal lines can be compared simply and simultaneously. In this sense, the T_m-diagram is somewhat analogous to the periodic table, in which all chemical elements are arranged simultaneously in a simple and systematic manner. Finally, my emphasis is that a simple molecular model can explain adequately the various shapes of the T_m-profiles exhibited by different series of mixed-chain phospholipids shown in this T_m-diagram. It is hoped that the experimental and computational results obtained with pure lipids containing well-defined numbers and positions of *cis*-double bonds as summarized in this presentation may lead us to many informative new experiments to be carried out with biological membranes in the future.

ACKNOWLEDGMENTS

This work was supported, in part, by U.S. Public Health Service Grant GM17452 from NIGMS, National Institutes of Health, and the Department of Health and Human Services. Sincere appreciation

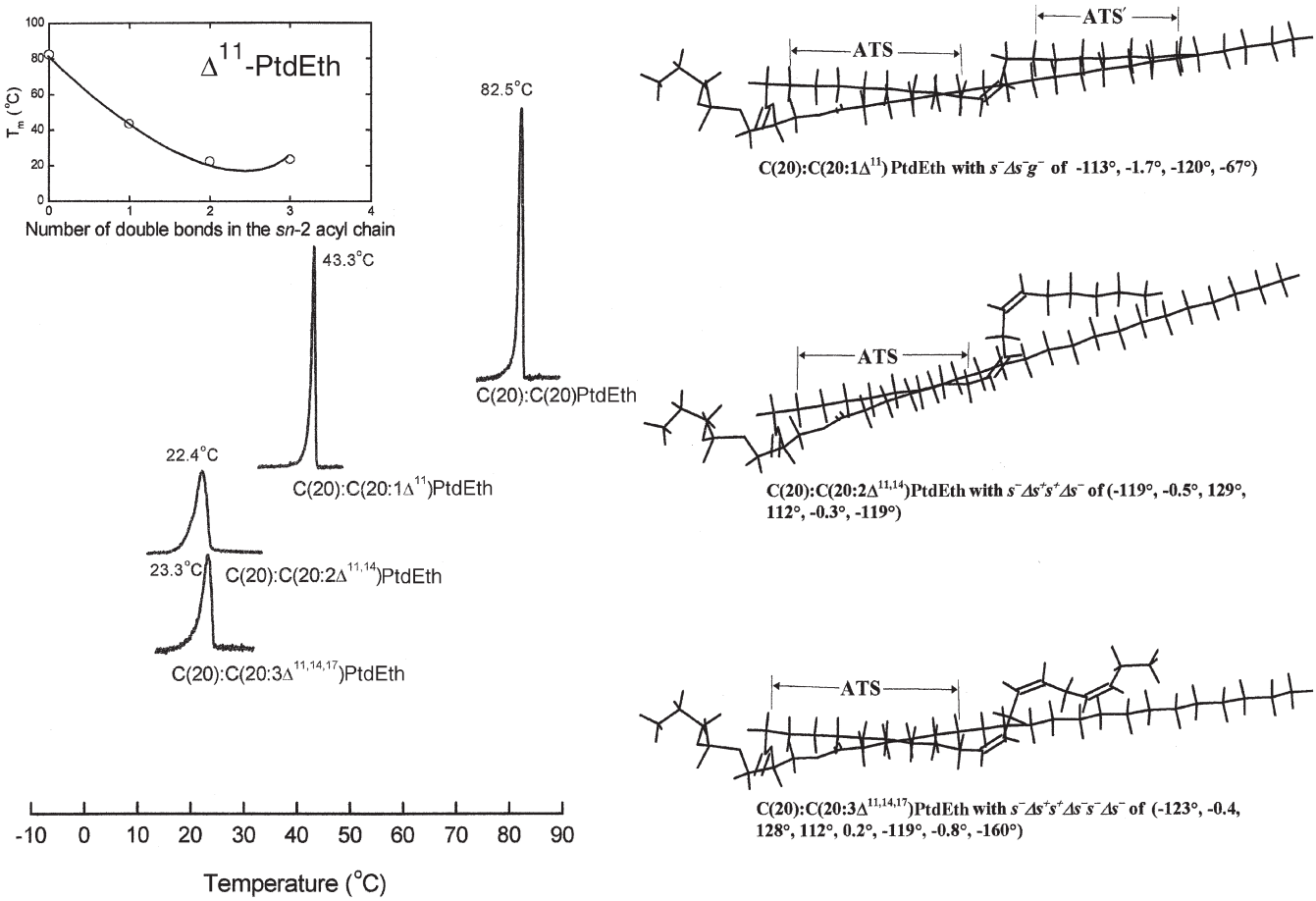

FIG. 22. The energy-minimized structures of the three lipids in the Δ^{11}PtdEth-series are shown in the presence of the down-and-up T_m-profile exhibited by these lipids.

is expressed to all the students, research associates, and collaborators whose work I have cited in this presentation. I am extremely grateful to Drs. Thomas E. Thompson, Robert G. Langdon, and James W. Ogilvie, who introduced me to the fertile field of membrane lipids while I was a graduate student as well as a junior faculty member. I would also like to express my deep appreciation to Drs. Rodney Biltonen, Joseph Larner, Ronald Taylor, and Thomas E. Thompson for their encouragement and appreciation. Finally, I thank my wife, Laura, and children, Tien-tsin and Tien-wei, for their continuous support during the long period of my research career.

REFERENCES

1. Huang, C. (1998) Membrane Lipid Structure and Organization, in *The Cell Physiology Source Book,* 2nd edn. (Sperelakis, N., ed.), pp. 39–60, Academic Press, New York.
2. Kennedy, E.P. (1986) The Biosynthesis of Phospholipids, in *Lipids and Membranes: Past, Present and Future* (Op den Kamp, J.A.F., Roelofsen, B., and Wirtz, K.W.A., eds.), pp. 171–206, Elsevier, Amsterdam.
3. Kunau, W.-H. (1976) Chemistry and Biochemistry of Unsaturated Fatty Acids, *Angew. Chem. Int. Ed. Engl. 15,* 61–74.
4. Chapman, D. (1993) Lipid Phase Transitions, in *Biomembranes: Physical Aspects* (Shinitzky, M., ed.), pp. 29–62, Balabon Publishers, Weinhein, Germany.
5. Thompson, T.E., Sankaram, M.B., and Huang, C. (1997) Organization and Dynamics of the Lipid Components of Biological Membranes, in *Handbook of Physiology, Section 14: Cell Physiology* (Hoffman, J.F., and Jamieson, J.D., eds.), Oxford University Press, pp. 23–56, Oxford.
6. Barton, P.G., and Gunstone, F.D. (1975) Hydrocarbon Chain Packing and Molecule Motion in Phospholipid Bilayers Formed from Unsaturated Lecithins. Synthesis and Properties of Sixteen Positions of 1,2-Dioctadecanoyl-*sn*-glycero-3-phosphorylcholine, *J. Biol. Chem. 250,* 4470–4476.
7. Hernandez-Borrell, J., and Keough, K.M.W. (1993) Heteroacid Phosphatidylcholines with Different Amounts of Unsaturation Respond Differently to Cholesterol, *Biochim. Biophys. Acta 1153,* 277–282.
8. Keough, K.M. (1990) Influence of Chain Unsaturation and Chain Position on Thermotropism and Intermolecular Interactions in Membranes, *Biochem. Soc. Trans. 18,* 835–837.
9. Koenig, B.W., Strey, H.H., and Gawrisch, K. (1997) Membrane Lateral Compressibility Determined by NMR and X-ray Diffraction: Effect of Acyl Chain Polyunsaturation, *Biophys. J. 73,* 1954–1966.
10. Litman, B.J., Lewis, E.N., and Levin, I.W. (1991) Packing Characteristics of Very Highly Unsaturated Bilayer Lipids: Raman Spectroscopic Studies of Multilamellar Phosphatidylcholine Dispersion, *Biochemistry 30,* 313–319.
11. Niebylski, C.D., and Salem, N., Jr. (1994) Calorimetric Investigation of a Series of Mixed-Chain Polyunsaturated Phosphatidylcholines: Effect of *sn*-2 Chain Length and Degree of Unsaturation, *Biophys. J. 67,* 2387–2393.

12. Sanchez-Migallon, M.P., Aranda, F.J., and Gomez-Fernandez, J.C. (1996) Interaction Between Alpha-Tocopherol and Heteroacid Phosphatidylcholines with Different Amounts of Unsaturation, *Biochim. Biophys. Acta 1279*, 251–258.
13. Huang, C., and Li, S. (1999) Calorimetric and Molecular Mechanics Studies of the Thermotropic Phase Behavior of Membrane Phospholipids, *Biochim. Biophys. Acta 1422*, 273–307.
14. Li, S., Lin, H., Wang, G., and Huang, C. (2001) Molecular Mechanics and Calorimetric Studies of Phosphatidylethanols, *Arch. Biochem. Biophys. 385*, 88–98.
15. Allinger, N.L., Yuh, Y.H., and Lii, J.-H. (1989) Molecular Mechanics. The MM3 Force Field for Hydrocarbons, *J. Am. Chem. Soc. 111,* 8551–8582.
16. Pearson, R.H., and Pascher, I. (1979) The Molecular Structure of Lecithin Dihydrate, *Nature 281,* 499–501.
17. Zaccai, G., Buldt, G., Seelig, A., and Seelig, J. (1979) Neutron Diffraction Studies on Phosphatidylcholine Model Membrane. II. Chain Conformation and Segmental Disorder, *J. Mol. Biol. 134*, 693–706.
18. Li, S., Lin, H., Wang, Z., and Huang, C. (1994) Identification and Characterization of Kink Motifs in 1-Palmitoyl-2-oleoylphosphatidylcholine: A Molecular Mechanics Study, *Biophys. J. 66,* 2005–2018.
19. Bultmann, T., Lin, H.N., Wang, Z.Q., and Huang, C.H. (1991) Thermotropic and Mixing Behavior of Mixed-Chain Phosphatidylcholines with Molecular Weights Identical with L-α-Dipalmitoylphosphatidylcholine, *Biochemistry 30*, 7194–7202.
20. Wang, Z.Q., Lin, H.N., and Huang, C.H (1990) Differential Scanning Calorimetric Study of a Homologous Series of Fully Hydrated Saturated Mixed-Chain C(X):C(X + 6) Phosphatidylcholines, *Biochemistry 29,* 7072–7076.
21. Wang, G., Lin, H.N., Li, S. and Huang, C.H. (1995) Phosphatidylcholines with *sn*-1 Saturated and *sn*-2 *cis*-Monounsaturated Acyl Chains: Their Melting Behavior and Structures, *J. Biol. Chem. 270,* 22738–22746.
22. Wang, Z.Q., Lin, H.N., Li, S., and Huang, C.H. (1994) Calorimetric Studies and Molecular Mechanics Simulations of Monounsaturated Phosphatidylethanolamine Bilayers, *J. Biol. Chem. 269,* 23491–23499.
23. McIntosh, T.J., Lin, H., Li, S., and Huang, C. (2001) The Effect of Ethanol on the Phase Transition Temperature and the Phase Structure of Monounsaturated Phosphatidylcholines, *Biochim. Biophy. Acta 1510*, 219–230.
24. Huang, C., Wang, G., Lin, H.N., and Li, S. (1998) A Unifying T_m-Diagram for Phosphatidylethanolamines with *sn*-1 C_{20}-Saturated and *sn*-2 C_{18}-Unsaturated Acyl Chains, *Biochim. Biophys. Acta 1373,* 282–288.
25. Wang, G., Li, S., Lin, H.N., Brumbaugh, E.E., and Huang, C. (1999) Effects of Various Numbers and Positions of *cis* Double Bonds in the *sn*-2 Acyl Chain of Phosphatidylethanolamine on the Chain-Melting Temperature, *J. Biol. Chem. 274,* 12289–12299.
26. Hitchcock, P.B., Mason, R., Thomas, K.M., and Shipley, G.G. (1974) Structural Chemistry of 1,2-Dilauroyl-DL-phosphatidylethanolamine: Molecular Conformation and Intermolecular Packing Phospholipids, *Proc. Nat. Acad. Sci. USA 71,* 3036–3040.
27. Ernst, J., Sheldrick, W.S., and Fuhrhop, J.-H. (1979) Die Strucktur der Essentiellen Ungesättigten Fettsäuren, Kristallstrucktur der Linolsäure Sowie Hinweise auf die Kristallstructuren der α-Linolensäure und der Arachidonsäure, *Z. Naturforsch. 346,* 706–711.
28. Wang, G., Li, S., Lin, H., and Huang, C. (1997) Influence of *cis* Double Bonds in the *sn*-2 Acyl Chain of Phosphatidylethanolamine on the Gel-to-Liquid Crystalline Phase Transition, *Biophys. J. 73,* 283–292.
29. Huang, C., Lin, H.N., Li, S., and Wang, G. (1997) Influence of the Positions of *cis* Double Bonds in the *sn*-2 Acyl Chain of Phosphatidylethanolamine on the Bilayer's Melting Behavior, *J. Biol. Chem. 272,* 21917–21926.

[Received May 16, 2001; accepted July 16, 2001]